Received: 22 October 2025 | Revised: 5 January 2026 | Accepted: 22 January 2026

DOI: 10.1002/dro2.70071

REVIEW ARTICLE

Droplet WILEY

Photothermal bubble: Dynamics, manipulation, and applications

Man Hu[1] | Feng Wang[2] | Daosheng Deng[1]

[1]Department of Aeronautics and Astronautics, College of Intelligent Robotics and Advanced Manufacturing, Fudan University, Shanghai, China

[2]Center for Combustion Energy, Department of Energy and Power Engineering, Tsinghua University, Beijing, China

Correspondence Daosheng Deng, Department of Aeronautics and Astronautics, Fudan University, Shanghai 200433, China.
Email: dsdeng@fudan.edu.cn

Funding information
National Natural Science Foundation of China, Grant/Award Number: 12572307; Shanghai Science and Technology Program, Grant/Award Number: 23ZR1403800; Postdoctoral Fellowship Program of the China Postdoctoral Science Foundation, Grant/Award Numbers: 2025T180524, GZB20240366, 2024M751637; Shuimu Tsinghua Scholar Program, Grant/Award Number: 2023SM038

Abstract

Photothermal bubble holds promising for microfluidics, microfabrication, drug delivery, chemical engineering, and soft robotics, arising from its inherent features and advantages, such as easy formation, remote operation, rapid response, tunable flexibility, and biocompatibility. This review systematically examines advances in photothermal bubble generation and manipulation over the past decade, focusing on nucleation mechanisms, growth dynamics, and motion control. Three principal modes of bubble motion are analyzed: horizontal locomotion driven by laser translation; spontaneous bouncing/oscillatory motion under stationary laser irradiation; and three-dimensional actuation via optimized heating configurations. We highlight representative applications demonstrating the versatility of photothermal-driven bubble manipulation, and discuss the related limitations associated with photothermal bubble actuation in various application scenarios. Furthermore, we present outlook for key challenges and future directions for broader implementation. This review offers fundamental insights into the underlying dynamics and control mechanisms of photothermal bubbles, facilitating the transition of this technology from laboratory research to practical applications.

INTRODUCTION

Bubbles have been recognized for their fundamental role both in natural phenomena and technological applications, due to their unique physicochemical properties and versatile functionalities.[1–4] For example, micro-nano bubbles, with high stability, adjustable size, and ability to generate free radicals, have emerged as a promising solution for green cleaning.[5,6] Air bubbles, generated and dispersed in pulps, have been widely used for mineral flotation by leveraging hydrophobic interactions and buoyancy effects.[7,8] Recent advances in interfacial science and bubble–particle interactions have catalyzed the development of sophisticated bubble-enabled technologies in cross disciplines.[9,10] In materials science, direct bubble writing has unlocked programmable fabrication of polymer foams with hierarchical architectures, where gas-core/liquid-shell structures are precisely patterned to tailor mechanical, thermal, and acoustic properties at multiple scales.[11,12] In microfluidics, bubbles serve as dynamic actuators, functioning as on-demand micropumps (via Marangoni flows or oscillatory expansion) and microvalves (through gas–liquid interface pinning), enabling precise fluidic control in lab-on-a-chip systems.[13–15] In biomedical engineering, innovations utilize bubbles as multifunctional platforms, including drug-loaded liposomes for targeted delivery,[16,17] acoustically propelled micromotors for noninvasive surgery,[18,19] and ultrasound contrast agents for enhanced imaging.[20,21]

The breakthroughs and advancements in bubble-based technologies have created an imperative for advancing fundamental research in bubble dynamics.[22–24] Especially, the precise control of bubble characteristics, such as size, stability, and spatial positioning, is critical for optimizing their performance in diverse applications. Two fundamental approaches have been developed for bubble manipulation: passive and active methods.[25,26] Passive techniques typically rely on engineered microstructured surfaces or chemical modifications to guide bubble behavior.[27] For instance, superhydrophobic surfaces with patterned wettability gradients can direct bubble movement,[28] while microcavity arrays can stabilize bubble size and position.[29] While passive trapping and control techniques provide distinct advantages in simplicity, low cost, and energy savings, their practical application is often constrained by limitations in manipulation flexibility and structural reconstruction.

In contrast, active methods utilize external energy inputs[30] (e.g., acoustic,[31–34] electric,[35,36] magnetic fields,[37–40] or optical excitation)[41–45] to dynamically control bubbles. Acoustic methods, which primarily employ ultrasonic or surface acoustic waves, offer the convenience of controlling multiple bubbles simultaneously, but selective manipulation of a single bubble remains challenging.[32] Electric field methods, which manipulate bubbles via dielectrophoresis or electrowetting, are ideal for high-speed and precise control; however, sequential processing requires complex electrode circuit designs and lacks reconfigurability.[46] For magnetic manipulation, bubbles must be loaded with magnetic nanoparticles or attached to magnetic beads, a process that may introduce contamination.[39] Optical methods, utilizing different laser sources through optical tweezers or the photothermal effect, offer the highest spatial resolution, allowing for precise trapping and manipulation of either single or multiple bubbles.[47] In particular, photothermal techniques, which are based on laser heating, have emerged as a particularly versatile platform for both bubble generation and manipulation.[48–50]

The photothermal effect usually relies on focusing laser light on photothermal materials (such as gold nanoparticles [GNPs] or carbon-based absorbers) to produce localized heating, which subsequently triggers vapor nucleation and bubble growth during laser irradiation.[51–54] This local heating also generates a surface tension gradient at the bubble–liquid interface, leading to a thermal Marangoni flow (or "thermocapillary flow") that effectively governs bubble motion.[55–58] Using the photothermal Marangoni effect, typical bubble motion modes—such as planar translation on a substrate,[59] periodic bouncing in bulk liquid,[60] and complex 3D motion from coupled flow forces[61]—have been demonstrated. Furthermore, multiplexed laser addressing via spatial light modulation or holographic techniques allows for the independent, versatile, and programmable control of multiple bubbles, thereby enabling parallel and high-throughput processing.[62]

In this review, we systematically examine recent progress in photothermal-mediated bubble dynamics, including the nucleation and growth dynamics of photothermal bubbles, the typical manipulation modes mediated by photothermal effects, and the representative applications of bubble-based technologies. The review is organized in terms of the bubble scenario, as illustrated in Figure 1. First, bubble generation via the localized photothermal effect is discussed. The designs and working principles and corresponding bubble dynamics are elaborated for two kinds of photothermal bubbles: surface bubble (including the "plasmonic bubble") and floating bubble. Then, we comprehensively summarize bubble manipulations mediated by photothermal effects in three cases: (i) the locomotion of surface bubbles driven by thermal-Marangoni flow; (ii) the periodic bouncing/oscillatory motion of bubbles via coupling bi-directional flows; (iii) the 3D dancing motion of floating bubbles realized by sophisticated laser heating designs. Lastly, we demonstrate bubble applications in microfluidic control, microrobots, microfabrication, and targeted drug delivery, and discuss the operational boundaries, stability limitations, and scalability challenges associated with photothermal bubble actuation. Perspectives regarding the future development of photothermal bubble manipulation and applications are outlined.

NUCLEATION AND GROWTH DYNAMICS OF PHOTOTHERMAL BUBBLES

When laser light irradiates an absorbing medium, the local temperature rises due to the photothermal effect, generating photothermal bubbles. If the wall or liquid is highly absorbing, typically with a laser penetration depth of several micrometers, the temperature increase is confined near the solid–liquid interface, as shown in Figure 2a, while the bulk liquid temperature remains nearly unaffected. Consequently, bubble nucleation occurs predominantly at the interface, forming a surface bubble. In contrast, when the wall is optically transparent to the laser and the liquid is moderately absorbing, with a penetration depth on the order of centimeters, the temperature rises along the laser path through the bulk liquid, as shown in Figure 2b. This enables bubble nucleation within the liquid, leading to the formation of a floating bubble. To compare these photothermal bubbles, Table 1 summarizes their operating conditions and physical mechanisms, which include the generation methods, bubble size, mechanisms, performance, and applications.

Nucleation mechanism of photothermal bubbles

In the absence of pre-existing nucleation sites, the surrounding liquid can become highly superheated, reaching temperatures well above its boiling point.[82] The theoretical limit of this superheating is the liquid spinodal temperature, indicated by the green solid line in Figure 2c.[71] However, classical nucleation theory (CNT) predicts that in practice, the presence of impurities or interfaces significantly lowers the required critical superheat. According to CNT, as the radius of a bubble nucleus increases, the system's free energy, composed of interfacial and volumetric contributions, exhibits a local maximum at a critical radius R_c, as shown in Figure 2d.[71] This maximum represents the thermodynamic energy barrier for nucleation. Overcoming this barrier requires the liquid to reach a specific superheat temperature, the so-called nucleation temperature T_n, which corresponds to a critical laser irradiation intensity. Upon exceeding the threshold laser intensity, a

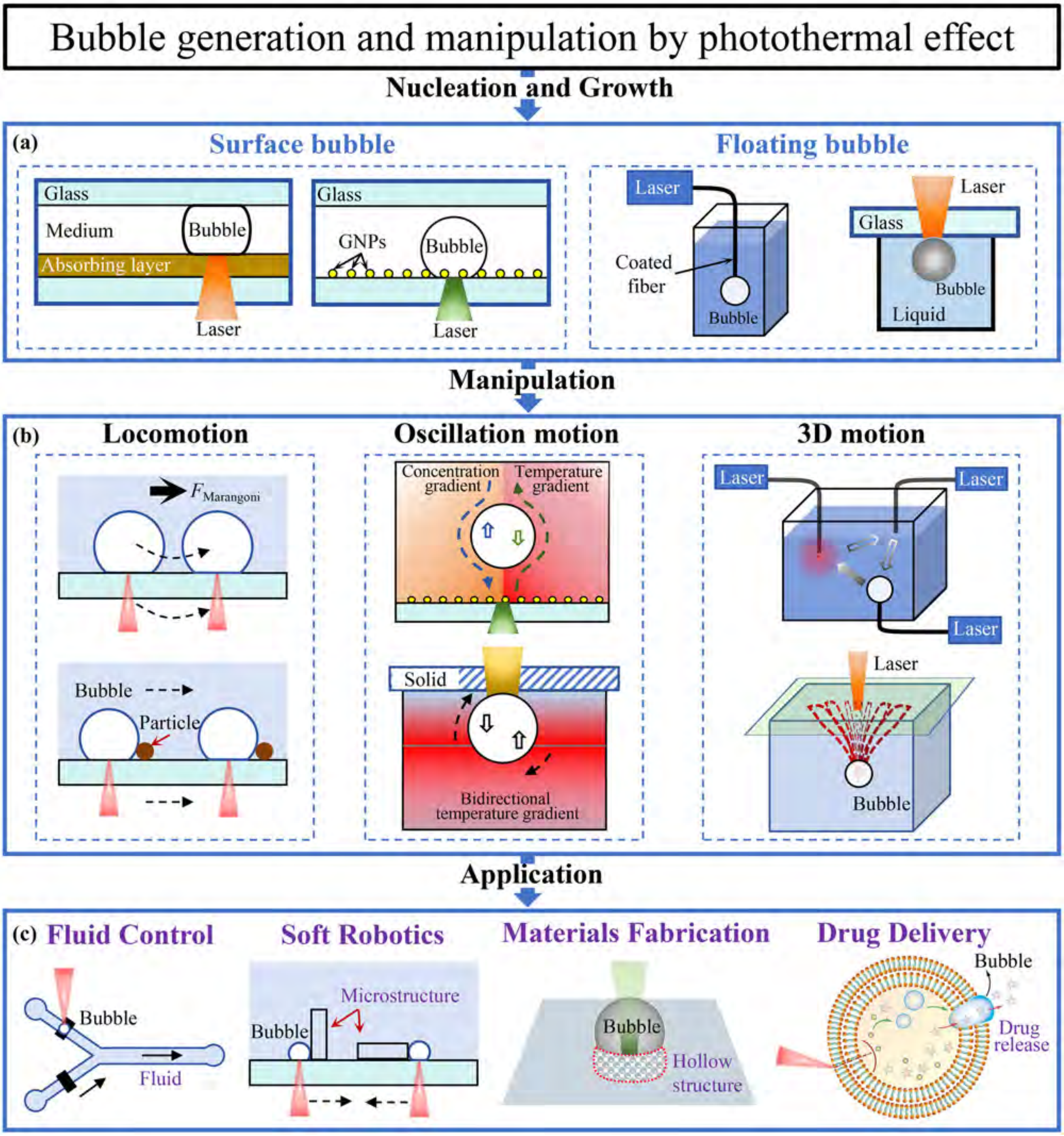

FIGURE 1 Manifestations of photothermal-mediated bubble generation, manipulation and application. (a) Illustration for two kinds of photothermal bubbles, including surface bubble and floating bubble. Reproduced with permission.[51, 63–65] Copyright 2017, Royal Society of Chemistry. Copyright 2014, American Chemical Society. Copyright 2012, Optical Society of America. Copyright 2022, Springer Nature. (b) Sketch for three typical cases for photothermal bubble manipulation, including locomotion motion, oscillatory motion, and 3D motion. Reproduced with permission.[61, 65–69] Copyright 2014, Springer Nature. Copyright 2016, American Chemical Society. Copyright 2021, National Academy of Sciences. Copyright 2022, Springer Nature. Copyright 2021, American Chemical Society. Copyright 2025, American Physical Society. (c) Exhibition for typical photothermal bubble-based applications in fluid control, soft robotics, materials fabrication, and drug delivery. Reproduced with permission.[49, 70–72] Copyright 2011, Royal Society of Chemistry. Copyright 2019, WILEY-VCH GmbH. Copyright 2024, Elsevier. Copyright 2021, AIP Publishing.

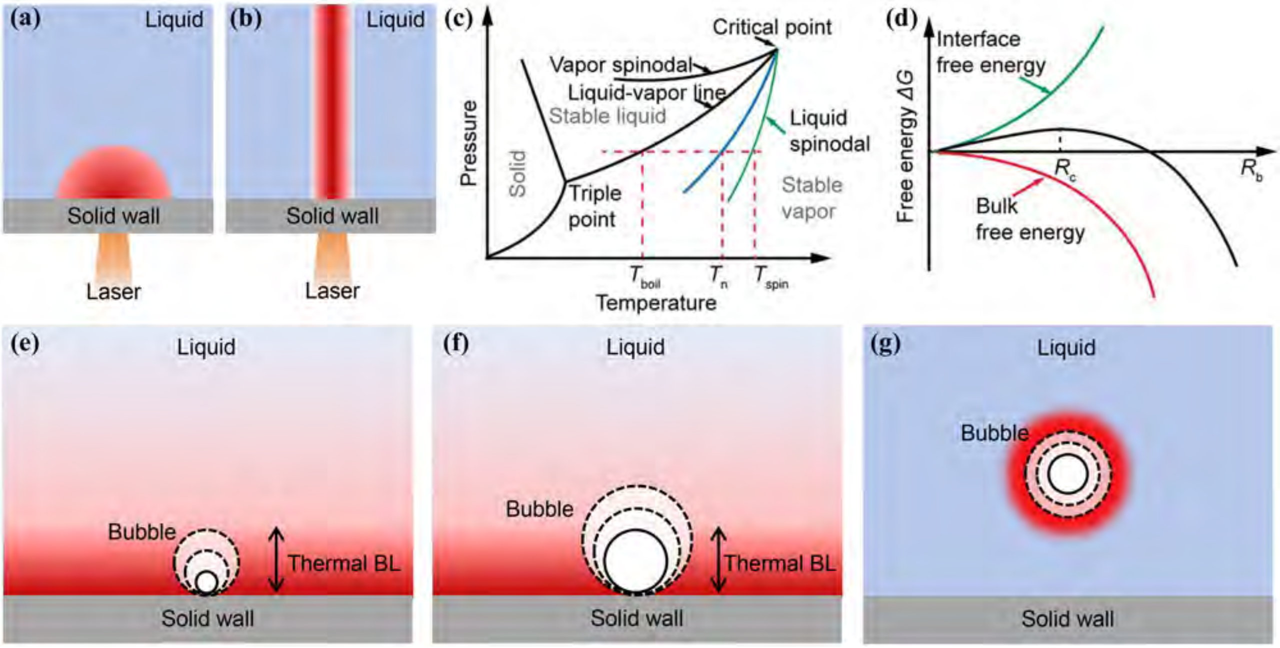

FIGURE 2 Physical mechanism of photothermal bubble nucleation and growth. (a,b) Schematic diagrams of the temperature distribution resulting from the laser-induced photothermal effect for (a) an absorbing solid or a highly absorbing liquid and (b) a moderately absorbing liquid. (c) Schematic phase diagram of water, indicating the theoretical liquid spinodal line (green solid line) and the experimentally measured nucleation temperature (blue solid line). (d) Free energy of homogeneous bubble nucleation as a function of the nucleus radius. Reproduced with permission.[73] Copyright 2024, Wiley-VCH GmbH. (e-g) Schematic diagram of photothermal bubble growth under different temperature distributions: (e) growth within the thermal boundary layer; (f) growth outside the thermal boundary layer; (g) growth under focused laser irradiation.

nucleus generated by density fluctuation will grow beyond the critical radius R_c, leading to the onset of photothermal bubble nucleation.

Thermally controlled growth mechanism of photothermal bubbles

The dynamics of a spherical bubble growing in an infinite liquid medium are often described by the well-known Rayleigh–Plesset equation.[82–84] This equation is derived from the conservation of mass and momentum (the Navier–Stokes equations) and takes the following generalized form:

$$\frac{p_b(t) - p_\infty(t)}{\rho_l} = R\frac{d^2R}{dt^2} + \frac{3}{2}\left(\frac{dR}{dt}\right)^2 + \frac{4\mu_l}{\rho_l R}\frac{dR}{dt} + \frac{2\sigma}{\rho_l R}, \quad (1)$$

where $p_\infty(t)$ and $p_b(t)$ are the pressures in the liquid far from the bubble and within the bubble, respectively. R, ρ_l, μ_l, and σ are the radius, density, dynamic viscosity, and surface tension of the liquid.

During the early, inertia-dominated stage of growth, viscous effects, surface tension, and the initial bubble radius can often be neglected. If the pressure difference $\Delta p = p_b(t) - p_\infty(t)$ remains approximately constant, Equation (1) reduces to an asymptotic form with a constant growth rate:

$$\dot{R} = \sqrt{\frac{2}{3}\frac{\Delta p}{\rho_l}}. \quad (2)$$

As the bubble grows larger, the rate of vaporization at the interface becomes limited by heat transfer. By balancing the conductive heat flux from the superheated liquid with the latent heat required for vaporization, the growth rate in this thermally controlled regime is given by[85, 86]:

$$\dot{R} = \frac{\rho_l c_{pl}(T_\infty - T_{sat})}{L\rho_v}\sqrt{\frac{3D_l}{\pi t}}, \quad (3)$$

where T_∞ and T_{sat} are the liquid temperature far from the bubble and the saturation temperature; c_{pl} and D_l are the liquid's specific heat and thermal diffusivity at constant pressure; ρ_v is the density of vapor; and L is the latent heat of vaporization.

Growth dynamics of surface bubbles

The growth dynamics of a photothermal bubble are strongly influenced by the surrounding temperature distribution,[87, 88] as sketched in Figure 2e–f. For a bubble sitting on the solid interface, if it is confined within the thermal boundary layer, its growth is primarily governed by the temperature evolution at the interface.[88] According to Equation (3), if the superheat $\Delta T = T_\infty - T_{sat}$ is constant, the bubble radius scales as $R \sim t^{1/2}$. More generally, if the superheat itself varies in time as $\Delta T \sim t^n$, the scaling becomes $R \sim t^{n+1/2}$. This asymptotic solution provides a good description for thermally limited growth when the bubble is immersed within the thermal boundary layer (Figure 2e) or

TABLE 1 Table for different photothermal bubbles.

Laser wavelength	Laser intensity (W/cm^2)	Medium	Mechanism	Bubble size (mm)	Bubble type	Performance	Application	Ref.
Visible (532 nm) or near-infrared (980 nm)	$1 \sim 10^5$	Absorbing surfaces (e.g., metal, silicon, Indium Tin Oxide, or their combinations)	Light absorption due to substrate materials	0.01 ~ 1	Surface bubble	Translation on substrates with arbitrary route	Fluid control, particle assembly, microrobot	Ref. 49, 70, 74, 75, 76, 77
532 nm	$10^5 \sim 10^7$	Gold nanoparticles	Localized surface plasmon resonance	0.001 ~ 0.1	Plasmonic bubble	Periodic bouncing	Material fabrication, micromanipulation, microrobot, clinical therapy	Ref. 54, 60, 63, 67, 68, 71, 78, 73, 79, 68, 71, 78, 73, 79
445 nm, 532 nm, 1064 nm	$\sim 10^3$	Nanoparticles coated optical fibers	Light absorption due to deposited nanoparticles	0.01 ~ 1	Fiber tip attached bubble to floating bubble	2D or 3D translation by adopting arrays of fibers	Micromanipulations, Microrobot	Ref. 61, 64, 80
980 nm	$\sim 10^3$	Absorbing liquids (e.g. water, ethanol, hexane)	Bulk light absorption	0.01 ~ 1	Floating bubble	1D bouncing, 2D hovering, or 3D orbiting	Particle assembly, material fabrication, microrobot	Ref. 65, 69, 81

at a laser spot (Figure 2g), where the thermal field is well-defined. Once the bubble diameter exceeds the thermal boundary layer thickness (Figure 2f), the dynamics are more complex that the growth is then governed by a nonuniform temperature field and a coupled interaction between thermal diffusion and vapor/gas diffusion.[63, 71, 87]

The growth dynamics of a surface photothermal bubble can be generated by using a continuous-wave (CW) near-infared laser light shone onto a chromium pad[49] (Figure 3a). Once the threshold laser power density (7.4 W/cm^2) is exceeded, the bubble nucleates and grows gradually. The volume of the bubble increases almost linearly with time, showing a power-three dependence between the bubble radius and time ($R^3 \propto t$). From the experimental evidence that the bubble keeps growing as long as the laser irradiation is maintained, and when the laser is turned off, the bubble shrinks but does not collapse, they deduce that the vaporization of the liquid and degassing of dissolved air, both contribute to the bubble growth. But further detailed analysis is not provided. Additional dynamics of a surface photothermal bubble was revealed by focusing a 405-nm laser onto a gold-coated substrate.[89] The bubble expansion rate shows the dependence on the laser power, with particularly rapid expansion occurring within the first 100 ms of illumination (Figure 3b). Notably, the experiments provide evidence for the gaseous (rather than vapor) nature of photothermal bubbles: Upon laser off, bubbles undergo gradual shrinkage due to the sudden temperature decrease but remain stable for extended periods (hours). This persistence contrasts sharply with the instantaneous collapse expected for vapor bubbles, fundamentally differentiating photothermal gas bubbles from conventional boiling phenomena.

In order to confirm the nature of the photothermal bubble, and the role of the dissolved gas in bubble dynamics, the evolution of a photothermal bubble in plasmonics was studied under CW illumination.[63] Compared to the heating of an absorbing surface with a focused laser beam where the heating area is diffraction-limited, illuminating a plasmonic nanostructure (noble metal nanoparticles) with a laser beam at their plasmonic resonance wavelength can confine the heat at the nanoscale, which makes the bubble generation more efficient and controllable.[51, 73] The generated surface bubbles due to the plasmonic resonance is referred as "plasmonic bubbles." To investigate bubble dynamics, a region approximately 7 μm in diameter was heated for 20 s to generate a bubble under steady-state conditions (Figure 3c). This steady state is characterized by a gas molecule depletion at the vicinity of the bubble during heating, but upon stopping heating (during the bubble shrinkage), a molecule accumulation is observed around the bubble. Based on the assumption that the bubble dynamics is governed by a diffusion process of the gas molecules in the liquid, considering that the pressure difference across the bubble interface (i.e., between the gas (P) and liquid (P_∞) pressures) is governed by the Young–Laplace equation as $P - P_\infty = 2\sigma/R$ (where σ is the surface tension of the gas–liquid interface), and assuming the ideal gas condition ($PV = NR_gT$, where $V = 4\pi R^3/3$ is the bubble volume, N is the amount of gas molecules (in moles), R_g is the gas constant, and T is the bubble temperature), the bubble radius evolution during the bubble shrinkage

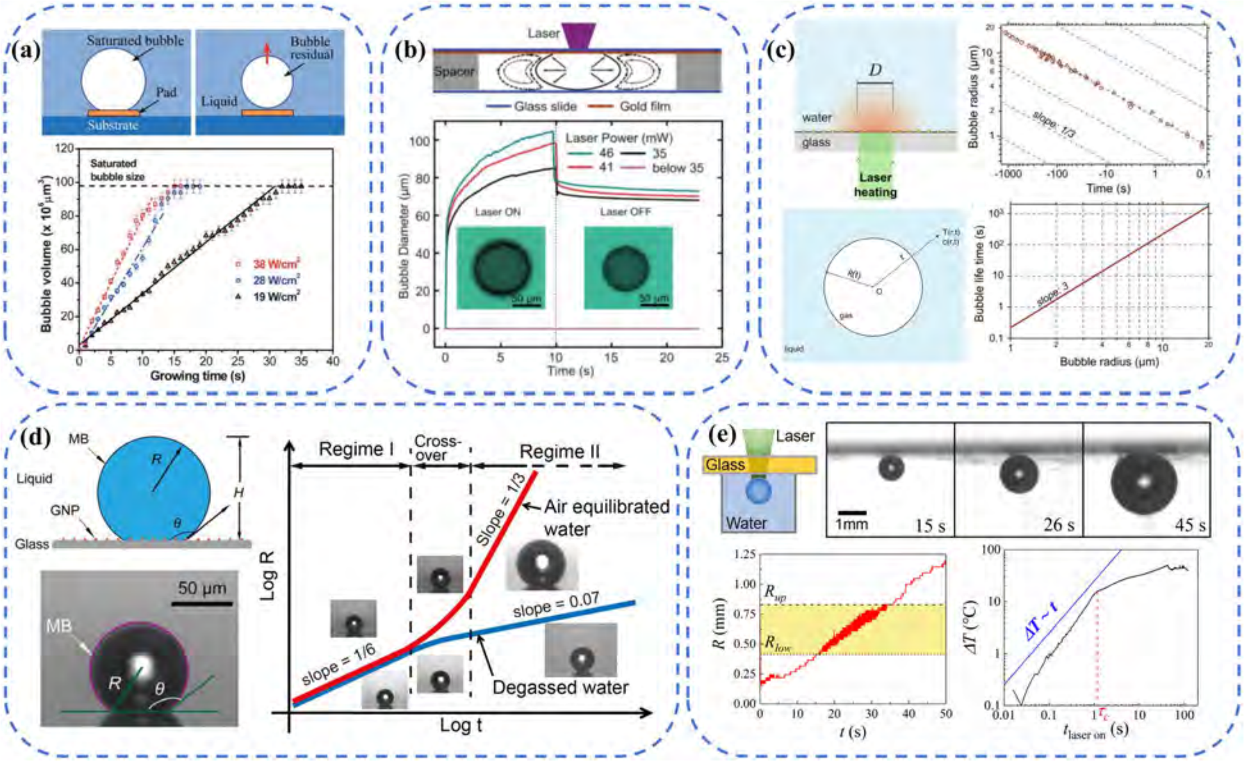

FIGURE 3 Growth dynamics of photothermal bubbles generated at absorbing substrates. (a) Dynamics of a surface bubble on an absorbing pad under the irradiation of a 980 nm laser. Reproduced with permission.[49] Copyright 2011, Royal Society of Chemistry. (b) A surface bubble formed on a gold coated glass coverslip. Reproduced with permission.[89] Copyright 2013, Royal Society of Chemistry. (c) The radius evolution and lifetime of a plasmonic bubble. Reproduced with permission.[63] Copyright 2014, American Chemical Society. (d) The growth dynamics of a plasmonic bubble for air-equilibrated water and degassed water. The bubble growth process can be divided into two phases with a crossover in between. Reproduced with permission.[78] Copyright 2017, American Chemical Society. (e) Dynamics of a photothermal floating bubble. The linear growth of bubble radius is interpreted by the scaling evolution of temperature $\Delta T \sim \sqrt{t}$. Reproduced with permission.[65] Copyright 2022, Springer Nature.

is derived[63]:

$$\frac{dR}{dt} = -\frac{2\sigma D R_g T}{KR^2\left(P_\infty + \frac{4\sigma}{3R}\right)}, \tag{4}$$

where D is the diffusion coefficient, K is the Henry's law constant of the gas. For long-lived bubbles that are at least a few micrometers in radius, the term $4\sigma/3R$ can be discarded.[90] In this approximation, the solution of Equation (4) reads:

$$R(t)^3 = -\frac{6R_g TD\sigma}{P_\infty K} t + const. \tag{5}$$

The scaling relation of $R \sim -t^{1/3}$ is evidenced experimentally (Figure 3c), which reveals that the bubble is not made of water vapor but of air molecules coming from the liquid. Also, the lifetime of the bubble can be simply estimated as $\tau = \frac{P_\infty K}{6R_g TD\sigma} R^3$.

In addition to the shrinkage dynamics of photothermal surface bubbles, the growth dynamics of plasmonic bubbles was investigated, clarifying the distinct contributions of vapor and dissolved air to the growth process.[78] The growth dynamics can be divided into two regimes: an initial short nucleation phase (regime I, < 10 ms) and subsequently a much longer growth phase (regime II) (Figure 3d). The bubble radius in the initial regime I scales with time as $R(t) \sim t^{1/6}$ by considering that the laser heating is mainly consumed by the evaporation of water and the heating efficiency decreases with the increasing of bubble volume, and the scaling law matches well with the experimental finding of $R(t) \propto t^{0.16}$. The identical growth rate for bubble in air-equilibrated water and degassed water observed experimentally further implies that the initial bubble growth in regime I is dominated by explosive vaporization of water. The long-term bubble dynamics in regime II is precisely described by the production-limited growth model[90] that predicts the bubble radius as $R(t) \sim t^{1/3}$ by considering the local oversaturation and the mass diffusion of the dissolved gas. The diffusion-controlled bubble growth rate is consistent with the shrinkage rate,[63] implying that the dissolved air plays a crucial role in the long-term bubble dynamics.

Growth dynamics of floating bubbles

Although surface bubble dynamics are now well understood, research on floating bubbles in the liquid phase is less advanced, as their inherent instability under normal conditions hinders systematic study. Microbubble can be produced by immersing tip-coated fibers in liquids.[64] Carbon nanoparticles are deposited onto the fiber end-face due to thermophoresis and pressure gradients via immersing the fiber in a solution of nanoparticles dispersed in ethanol and launching a laser beam through the waveguide.[91,92] Light absorption by the nanoparticles provides an extremely localized area over which thermal fluctuations lead to spontaneous formation of bubbles as a result of vaporization of the liquid. The bubble grows until reaching a maximum size, and then detaches from the fiber tip once the buoyancy force exceeds the "attachment" force $2\pi R_F \sigma$ (where R_F represents the effective size of the area covered by nanoparticles onto which the bubble is being formed). In fact, this floating bubble is essentially the same as the plasmonic bubble described above, but due to the small contact area between the bubble and the fiber tip, the bubble experiences weak adhesion and is more likely to detach from the contact surface and float in the liquid phase, allowing for 2D or 3D manipulations.[61,80,93,94]

To investigate the growth dynamics of floating bubble nucleated in the bulk liquid through liquid absorbing, our group introduced a type of laser heating by using a medium power near-infrared (NIR) laser (with a wavelength of 980 nm) to impact on pure water (Figure 3e).[65] Due to the absorption coefficient of 0.45/cm at 980 nm wavelength for water, a vapor bubble is formed underwater at an elevated temperature, once the laser power exceeds the threshold value (1.9 kW/cm^2). During the bubble growth within 50 s, the bubble radius has a tendency to increase linearly with time, which is different from both the 1/6-power law dominated by explosive evaporation, and the 1/3-power law dominated by mass diffusion of the dissolved gas due to local oversaturation. We interpret the linear growth of bubble radius by the scaling evolution of temperature $\Delta T \sim \sqrt{t}$. According to the Plesset–Zwick approximation for thermal controlled growth of bubble,[82] if the temperature obeys $\Delta T \sim R^* t^{n-0.5} C(n)$, then the bubble radius takes the form $R = R^* t^n$, where $C(n)$ is a constant for specific n. Our experiments are for the case $n = 1$.

MULTIMODE MANIPULATIONS OF BUBBLES

Since both surface and floating bubbles exhibit extended lifetimes under CW laser irradiation, their diverse manipulation for a wide range of applications can be achieved by harnessing photothermally induced flows and long-range hydrodynamic forces. This section summarizes three typical bubble motion modes enabled by laser heating: the 1D or 2D locomotion of surface bubbles, the periodic bouncing or oscillation of plasmonic and floating bubbles, and the 3D dancing and orbiting of floating bubbles. We focus on these three types of photothermally driven manipulation and discuss the underlying mechanisms of the respective strategies.

Physical mechanism of bubble motion driven by photothermal effects

When a laser irradiates a liquid, it generates complex temperature distributions and flow fields, leading to intricate bubble motion due to photothermal effect. The local heating of absorbing substrates usually creates a thermal gradient along the bubble–liquid interface. This thermal gradient affects the surface tension of the liquid, as most liquids have a negative constant value of $\partial\sigma/\partial T$, where σ is the surface tension and T is the temperature. Thus, the presence of a temperature gradient will decrease the surface tension in the warmer region and create a flow toward the colder region, as the liquid attempts to minimize the total surface energy, known as thermocapillary flow or thermal Marangoni flow.[47] The forces governing bubble motion in such a configuration are primarily the buoyancy force F_b, the Stokes drag force F_v, and the thermal Marangoni force F_m, as shown in Figure 4a–c.

The buoyancy force (Figure 4a) arises from the hydrostatic pressure in the fluid:

$$F_b = \frac{4}{3}\pi R_b^3 \rho_l g, \tag{6}$$

where R_b is the radius of the bubble, ρ_l is the density of the liquid, and g is the gravitational acceleration.

The Stokes drag force (Figure 4b) is induced by liquid viscosity and depends on the relative velocity between the bubble and the surrounding liquid:

$$F_v = 6\pi\mu R_b v, \tag{7}$$

where μ is the dynamic viscosity and v is the relative speed of a bubble to the surrounding liquid.

In a temperature field with a uniform gradient, bubbles in the liquid driven by thermal Marangoni flow experience a net movement toward the high-temperature regions,[55] as shown in Figure 4c. This force can be estimated by[82]

$$F_m = 2\pi R_b^2 \frac{d\sigma}{dT}\frac{dT}{dx}. \tag{8}$$

In practice, when a laser vertically irradiates a liquid, the resulting temperature distribution can trigger natural convection in the bulk liquid, as shown in Figure 4d. This establishes an axisymmetric stagnation point flow with associated viscous and thermal boundary layers. In this configuration, the coupling of forces across different coordinates must be considered. A schematic of the typical force balance is depicted in Figure 4e. By decomposing the forces in each coordinate, the bubble's motion along principal directions can be determined, ultimately enabling the prediction of its three-dimensional trajectory.

1D and 2D locomotion of bubbles driven by the thermal Marangoni flow

For bubbles in liquid, the optically induced temperature gradient results in a net movement of the bubble toward the warmest location, which corresponds to the position of the laser beam spot. In other words, the bubble can be easily navigated by translating or scanning the laser spot.

An optically actuated thermal Marangoni force, generated by local laser heating of an absorbing substrate, can trap and transport air

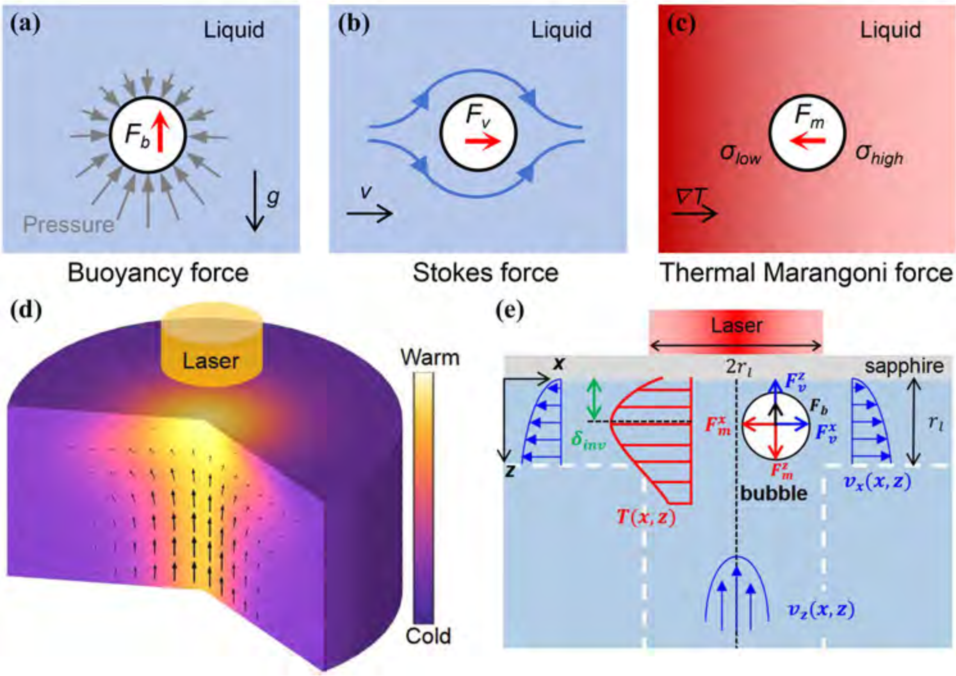

FIGURE 4 Physical mechanism of bubble motion driven by photothermal effect. (a–c) Schematic diagrams of forces acting on a bubble: (a) buoyancy force due to hydrostatic pressure; (b) stokes drag force from relative motion between the bubble and the surrounding liquid; (c) thermal Marangoni force arising from a surface tension gradient induced by a temperature gradient. Reproduced with permission.[73] Copyright 2024, Wiley-VCH GmbH. (d) Simulated temperature distribution and flow field under vertical laser irradiation of the liquid. Reproduced with permission.[81] Copyright 2024, National Academy of Sciences. (e) Force analysis of a floating photothermal bubble in the configuration shown in (d). Reproduced with permission.[69] Copyright 2025, American Physical Society.

bubbles (Figure 5a).[59] A bubble follows a laser spot scanned across the substrate, and its maximum transport velocity scales linearly with laser intensity, as the intensity generates the magnitude of the induced thermal gradient. Simulations verify that temperature and surface tension gradients drive a horizontal flow from the hot to the cold side of the bubble, propelling it toward the heated region (Figure 5b).[95] Moreover, a bubble centered over a symmetric thermal gradient is stably trapped. Here, the horizontal Marangoni flow vanishes, but a vertical temperature gradient establishes a convective flow. This induced circulation, perpendicular to the substrate, facilitates particle micromanipulation.

Laser heating can be used to directly generate thermal bubbles, rather than injecting air bubbles into the fluidic chamber. Consequently, the size and movement of the bubble can be flexibly controlled by adjusting the exposure time and the location of the laser. A low power weakly focused CW laser (532 nm) was applied to create a thermal bubble on a silver film.[74] By moving the laser spot, the location of the bubble is easily manipulated, allowing the direct-writing of micropatterns on the substrate with accumulated particles (Figure 5c). A thermal bubble generated by a CW laser (405 nm) irradiating on a gold-film–coated substrate demonstrated a different approach to particle manipulation, whereby particles carried by the bubble could be precisely guided along a predefined path (Figure 5d).[76]

The motion of particles can be analyzed by considering long-range forces (the drag force arising from the convective flow) and short-range forces (surface tension and pressure forces, van der Waals force) simultaneously. When particles are introduced into a flow field around a photothermal bubble, the particles are first driven toward the bubble surface by the heat-induced convective flow, and then trapped on the bubble's surface by a balance of a surface tension force and a pressure force.[76] This combination of forces enables the attraction of particles that are both near and far away from the bubble and the manipulation to any predefined location.

However, it should be noted that if the force balance between surface tension and pressure force is not satisfied, particles will be pushed away from the bubble at the ceiling and squeezed to the bubble at the floor. At the corner between the bubble and substrate, the particles are attracted to the substrate by the short-range van der Waals force.[74] This feature facilitates a new micro-lithography technique called "bubble-pen lithography," which uses the bubble as a pen to directly write patterns with micro- or nano-sized particles.[67,96,97] As shown in Figure 5e, the bubble can be generated due to the plasmon-enhanced photothermal effects and captures and immobilizes the colloidal particles on the substrate through coordinated actions of Marangoni convection, surface tension, gas pressure, and substrate adhesion. Through translating the laser beam to move the bubble, arbitrary single-particle patterns and particle assemblies with different resolutions and architectures can be created.

To improve the efficiency of manipulation, parallel generation and transportation of microbubbles can be achieved by creating multiple localized optical patterns using optical elements such as

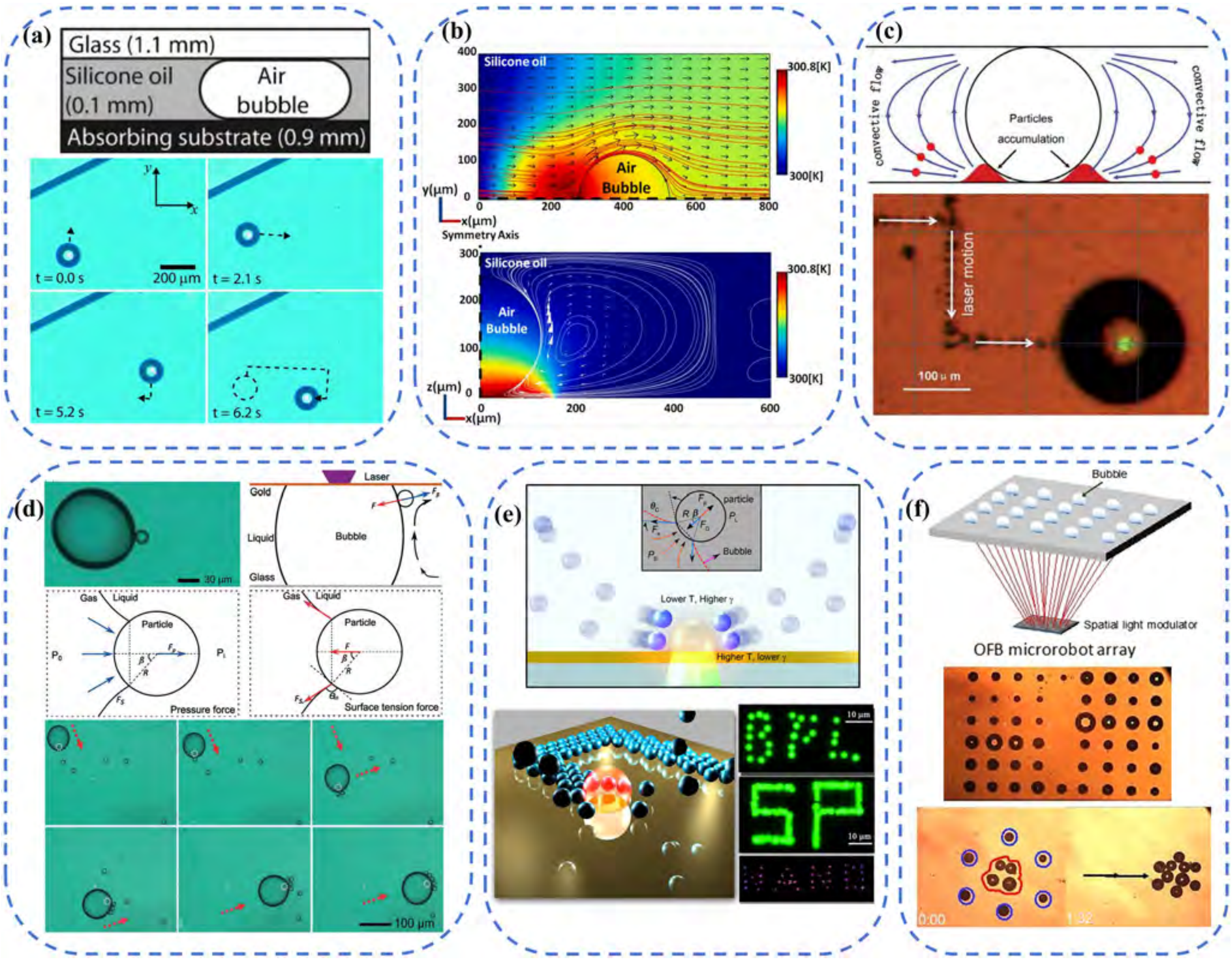

FIGURE 5 The locomotion of bubbles driven by thermal Marangoni flow. (a) Optically actuated thermal Marangoni movement of an air bubble in silicone oil. The bubble follows the position of the laser spot, as it is scanned in the *xy*-plane. Reproduced with permission.[59] Copyright 2007, AIP Publishing. (b) The simulated flow field around a bubble. Reproduced with permission.[95] Copyright 2011. AIP Publishing. (c) The direct-writing of micropatterns by manipulation a thermal bubble by moving the laser spot. Reproduced with permission.[74] Copyright 2011, Royal Society of Chemistry. (d) The demonstration of particle-manipulation that particles can be attracted to the bubble and then be precisely controlled by moving the bubble along a prescribed route. Reproduced with permission.[76] Copyright 2014, Royal Society of Chemistry. (e) Schematic and Working principle of bubble-pen lithography. Reproduced with permission.[67] Copyright 2016, American Chemical Society. (f) The cooperation of multiple bubbles by using a spatial light modulator to improve the manipulation efficiency. Reproduced with permission.[62] Copyright 2017, Springer Nature.

micromirrors,[98] spatial light modulators,[99] or scanning mirrors.[100] Hu et al.[66] designed an interactive control system with a scanning mirror and a touch screen interface to achieve matrix assembly of polystyrene particles by four thermal Marangoni flow–driven bubbles. Figure 5f shows collaborative microscopic manipulation by using 50 independently driven bubbles.[62] To activate up to 50 microbubbles, a single laser beam is split into 50 spots focused on the absorbing layer of the substrate by using a programmable spatial light modulator. The parallel, independent actuation of each bubble in a different direction is achieved, and actuation of pairs and groups of bubble-based microrobots in various trajectories is demonstrated.

Periodic bouncing/oscillatory motion driven by combined photothermal and gravitational fields

The manipulation of bubbles and bubble-based microrobots is typically restricted to 2D translation, owing to their formation and actuation on substrate surfaces. The resulting motion is dictated by the balance between the thermally generated Marangoni force and the bubble–substrate interfacial forces. An asymmetric thermal force weaker than the interfacial forces results in inefficient driving. Moreover, adhesive resistance from the substrate typically limits transportation speeds to hundreds of micrometers per second. To diversify manipulation modes and improve performance, strategies enabling substrate-detached motions—like vertical bouncing or oscillation—have been developed.

This section primarily reviews the periodic bouncing/oscillatory motion of photothermal bubbles. Such vertical motion is generally governed by the competition between several dominant opposing forces, including buoyancy, the thermal Marangoni, and Stokes' drag force. To facilitate bubble detachment from surfaces, strategies such as using hydrophilic substrates or optical fiber tips (which minimize contact area) are often utilized, enabling the driven forces to readily release the bubbles.

As demonstrated in Figure 6a, the controllable bubble bouncing motion was realized on a GNP decorated surface with a hydrophilic silica coating.[60] When GNPs are irradiated by a CW laser at their resonance frequency, a huge amount of heat is rapidly produced due to the plasmonic effect, a plasmonic bubble nucleates and grows on the surface during the laser-on period. After the laser is switched off, the plasmonic bubble detaches through the wetting of the substrate and rises upward driven by the buoyancy force. The bubble can then be pulled back to the substrate by the thermal Marangoni force once the laser is switched on. This rising and falling motion is governed by the competition between forces, including the buoyancy force, the thermal Marangoni force, the added mass force, and the Stokes' drag force, which can be described by the following equation [60]:

$$F = -\frac{10}{3}\pi\rho R_b^3 \ddot{z}(t) - 6\pi\rho\nu R_b \dot{z}(t)\left(1 + \frac{R_b}{z(t)}\right) + \frac{4}{3}\pi\rho R_b^3 g + 2\pi R_b^2 \frac{\partial\sigma}{\partial T}\frac{\partial T}{\partial z}, \quad (9)$$

where $z(t)$, $\dot{z}(t)$, and $\ddot{z}(t)$ are the displacement, velocity, and acceleration of the bubble. The four terms on the right side of the equation are the added mass plus liquid acceleration, Stokes' drag force, buoyancy force, and the thermal Marangoni force. The initial acceleration process of the bubble is influenced by the added mass force, while the rising in the bulk solution is subjected to buoyancy and drag forces. Once the laser is turned on, the bubble moves back to the substrate due to the thermal Marangoni force.

Besides the active modulation of the incident laser, the vertical bouncing motion of bubbles can also be spontaneously triggered via competition of solutal and thermal Marangoni forces in binary liquids. The periodic bouncing of a plasmonic bubble has been reported in a water/ethanol binary liquid (Figure 6b).[68] Once a bubble touches the hot substrate, the selective vaporization of ethanol near the substrate causes a downward Marangoni flow at the bubble interface, pushing the bubble upward. For a rising bubble, the solutal Marangoni force decreases more rapidly with increasing bubble height, and the thermal Marangoni force dominates bubble motion. Then, the bubble is pulled back to the substrate. This process repeats and the bubble can bounce for several dozens of cycles. The forces acting on the bouncing bubble can be described by Equation (9) by including the solutal Marangoni force $F_{s-M} = 2\pi R_b^2 \frac{\partial\sigma}{\partial c}\frac{\partial c}{\partial x}$, where c is the solute concentration. For applications, the bouncing dynamics of bubbles in multicomponent liquids give insights into the improvement of efficiency in processes like electrolysis and catalysis.[103]

In photoelectrochemical (PEC) water splitting, bubble formation and coverage on the photoelectrode reduce the effective electrode–electrolyte contact area, lowering reaction efficiency—an effect that intensifies as bubbles grow.[104] Bubble bouncing and rising near the surface can enhance heat transfer, and bubble collisions can improve local mass transfer, thus increasing chemical reaction efficiency. Light-chopping technology was employed to achieve bubble bouncing on a TiO_2 photoelectrode (Figure 6c).[101] By modulating the laser on/off times, they directionally regulated the bouncing characteristics. This chopping approach significantly shortened bubble growth time and reduced detachment diameter compared to continuous illumination. Additionally, coalescence-induced bubble jumping/detachment has been explored.[105] Using the thermal Marangoni effect to drive bubble sliding and coalescence, jumping occurs upon the release of surface energy. For smaller bubbles, jumping rather than full detachment is often observed, as their weaker buoyancy and lesser surface energy release hinder permanent departure from the electrode.

For thermally generated floating bubbles at the optical fiber tip, bouncing behaviors can be implemented by heating liquids with another optical fiber deposited with nanoparticles. The 2D bouncing manipulation of photothermal bubbles in ethanol by using two optical fibers has been investigated (Figure 6d).[80] The generation of a bubble on the fiber tip is carried out by allowing the passage of beam B (A) while beam A (B) is obstructed. Once the bubble is created, beam B (A) is obstructed and beam A (B) is allowed to pass, heating up the other fiber tip. The bubble is affected by the temperature gradient on the opposite fiber tip and is attracted toward it. The periodical bouncing manipulation in 2D of the floating bubble between two vertically or horizontally placed fibers can be realized by alternately lighting one of the fibers.

Despite the remarkable progress in bouncing bubbles, the exquisite manipulation of bubbles in pure liquids by decorating the thermal flow field with simple apparatus remains largely unreported. Recently, by introducing a thermally conductive interface, our group observed the spontaneous periodic bouncing motion of a photothermally generated floating bubble within pure water (Figure 6e).[65] The nucleation and growth of this floating bubble occurs underwater due to the volumetric absorption of 980 nm laser by pure water. A highly conductive sapphire glass is used as a coverslip to rapidly dissipate the heat near the solid cover, which results in the unique formation of a temperature inversion layer (TIL). The depth-dependent bi-directional thermal Marangoni force originated from the formation of TIL is responsible for the bouncing behavior. When the bubble rests near the cover, the downward Marangoni force acts as the driving force to push the bubble away from the solid wall. However, it will be pulled back driven by the upward thermal Marangoni force and buoyancy force when they are far away from the TIL. As a result, the bubble bounces along the vertical direction near the hot spot. The bouncing regime, defined by the lower and upper bound radii (R_{low} and R_{up}), and its frequency are derived from a force balance among buoyancy, downward Marangoni force, and upward Marangoni force. A fascinating dancing motion of the floating bubble was revealed by translating the laser spot horizontally, as

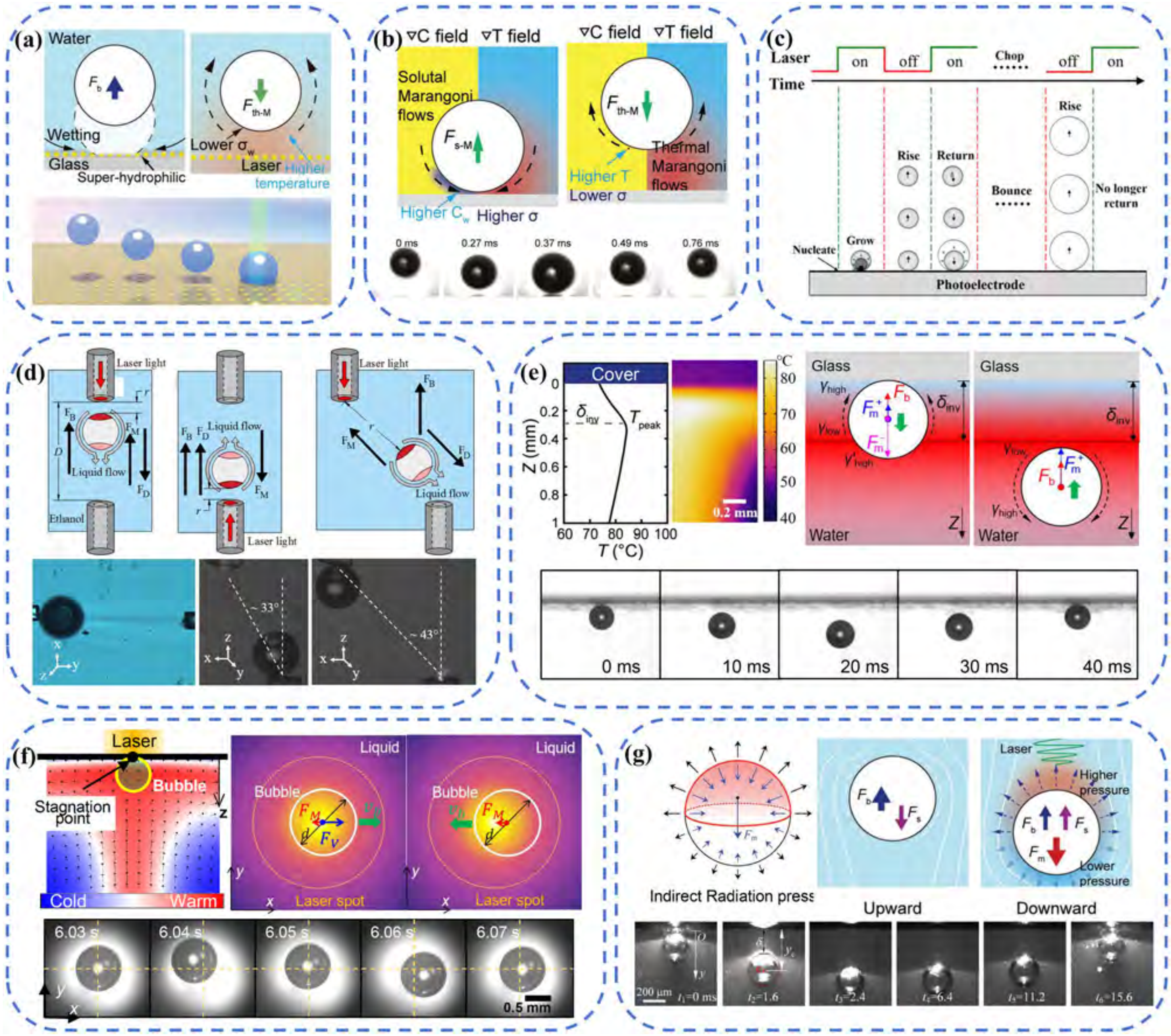

FIGURE 6 The periodic bouncing/oscillatory motion of bubbles driven by photothermal effects. (a) Plasmonic bubble bouncing behavior during laser on and off on gold nanoparticle-decorated surfaces with a hydrophilic silica coating. Reproduced with permission.[60] Copyright 2023, Wiley-VCH GmbH. (b) Periodic bouncing of a plasmonic bubble in an ethanol–water binary liquid due to the competition of solutal Marangoni force and thermal Marangoni force. Reproduced with permission.[68] Copyright 2021, National Academy of Sciences. (c) Bubble bouncing behavior regulated by laser chopping mode on a horizontal photoelectrode surface. Reproduced with permission.[101] Copyright 2022, American Chemical Society. (d) Manipulation of a microbubble between two vertically or horizontally opposed and off-axis optical fibers due to the switching of the temperature gradients. Reproduced with permission.[80] Copyright 2018, Optical Society of America. (e) Vertical bouncing motion of a floating photothermal bubble due to the competition between the bi-directional thermal Marangoni force and the buoyancy force. Reproduced with permission.[65] Copyright 2022, Springer Nature. (f) Spontaneous horizontal oscillatory motion of a photothermal bubble by impacting a laser on ethanol. The viscous driving force and the restoring thermal Marangoni force are responsible for the oscillation. Reproduced with permission.[81] Copyright 2024, National Academy of Sciences. (g) Bubble bouncing caused by the competition between buoyancy, indirect radiation pressure, and Stokes force. Reproduced with permission.[102] Copyright 2020, WILEY-VCH GmbH.

discussed in Section "3D dancing motion of bubbles via sophisticated designing of laser heating."

The advantage of this volumetric laser heating system is that the thermally induced flow field can be modulated by changing the liquid medium. When irradiating the 980 nm NIR laser into ethanol, a horizontal oscillatory motion mode of the photothermal bubble was identified by our group (Figure 6f),[81] instead of the vertical bouncing motion. By analyzing the temperature distribution and flow field around the bubble, the vertical bouncing motion is suppressed due to the relative large upward viscous drag force compared with that in water. The occurrence of horizontal oscillatory motion is due to the competition between the restoring horizontal thermal Marangoni force and the disturbing viscous drag force, since the temperature is higher at the center, the horizontal thermal Marangoni force tends to stabilize or trap the bubble at the center, while the viscous drag force induced by the stagnation flow tends to sweep the bubble away from the center.

The expansion of bubbles can also lead to their bouncing motion. A novel mechanism called indirect radiation pressure is introduced, which drives the bouncing motion of floating plasmonic bubbles (Figure 6g).[102] The bulk plasmonic bubble is generated when a GNP suspension solution is irradiated by a laser. The bubble rises due to buoyancy and falls due to the indirect radiation pressure force F_m originating from asymmetric vaporization. Because the indirect radiation pressure force F_m is size dependent, the bouncing behavior of the bubble appears only when the F_m is larger than Stokes drag force and ends when the buoyancy dominates.

3D dancing motion of bubbles via sophisticated designing of laser heating

The preceding sections show that photothermal effects have established diverse techniques for 1D and 2D bubble manipulation. However, despite the challenges, achieving noninvasive and precise 3D trapping and control remains crucial for applications such as targeted drug delivery, microfluidics, and optofluidics.

Consider that the thermal Marangoni effect can induce large and long-range forces acting on bubbles, it is possible to realize 3D manipulation of bubbles via sophisticated designing of laser heating in bulk liquids. Based on the Marangoni force–driven manipulation of floating bubbles between two fiber ends,[80] Sarabia-alonso et al.[61] realized the 3D steady-state trapping and manipulation of bubbles in liquids by using an array of three fibers with deposited nanoparticles (Figure 7a). When all three optical fibers are illuminated with lasers, the bubble can be trapped in the middle of the fiber array. The 3D transfer of bubbles from one fiber to another is implemented by sequentially switching on and off the lasers. However, the invasion of optical fibers significantly reduces the benefits associated with optical manipulation of contactless.

For the sake of formation of TIL in our previous work,[65] the vertical bouncing of photothermal bubbles is obtained. By introducing another degree of freedom, that is, the horizontal translation movement of the laser beam, we realized the intriguing 3D dancing motion of the bubble, which not only presents the excellent steerability with the laser beam, but also preserves the bouncing behavior along the vertical direction (Figure 7b).[81] The horizontal translation of the bubble is driven by the thermal Marangoni force along the x direction to push the bubble toward the hotter area of laser beam, since the thermal gradient ($\frac{dT}{dx}$) arises from the local heating in the course of the translation. The preserved bouncing behavior subject to the translation is due to the temperature gradient $\frac{dT}{dz}$ along the z direction within TIL. By comparing the two timescales for the formation of $\frac{dT}{dx}$ (local dwelling timescale $\tau_d \sim 2r_l/v_l$, where r_l and v_l are the radius and translation speed of the laser beam) and $\frac{dT}{dz}$ (the characteristic timescale for the heat transfer τ_c), various trajectories of the bubble are demonstrated that bouncing dominates at a lower speed ($\tau_d > \tau_c$) while translation dominates at a higher speed ($\tau_d < \tau_c$). By taking advantage of the unique bouncing and steerability features of this dancing bubble, through the precise control of the specific interaction with the preexisting objects including walls, bubbles, droplets, or nanoparticles, we successfully demonstrate its versatile capability to leap over a wall, coalesce with bubbles, form the core(bubble)-shell (droplet) structure, and collect particles within water (Figure 7b), which shows significant application potential in soft robotics, materials manufacturing, and water treatment.

To further investigate the intrinsic influence of liquid physicochemical properties on bubble motion mode in the volumetric laser heating system,[65,81] by exploring the various liquid medium from ethanol to hexane, our group observed a spontaneous 3D-periodic orbiting motion mode of a photothermal floating bubble (Figure 7c), which extends the spectrum of multimode motions beyond the 1D and 2D paradigms.[69] As revealed in our previous works,[65,81] the 1D vertical bouncing mode of the bubble is produced in water by a downward thermal Marangoni force (F_m^z) and an upward viscous drag force (F_v^z), while the 2D horizontal oscillatory motion mode of the bubble in ethanol is induced when the viscous drag force from the stagnation flow (F_v^x) becomes dominant, and the thermal Marangoni force (F_m^x) acts as a restorative force. Particularly, the 3D-orbiting motion mode of the photothermal bubble in hexane is attributed to the subtle interplay between the interfacial flow due to the thermal Marangoni effect and the bulk flow from the thermal buoyancy effect, and it acts as a synergistic coupling mode between the 1D vertical bouncing mode and the 2D horizontal hovering mode. Generally, the multimode motions of the bubble within different liquids are determined by the force balance between the thermal Marangoni force ($F_m^i = \Delta\gamma_i d$, where $\Delta\gamma_i$ is the surface tension gradient, and d is the bubble diameter) and the viscous drag force ($F_v^i = 6\pi\mu v_i d$, where v_i is the relative velocity between the bubble and the surrounding liquid along the i-direction) along each axis, thus a phase diagram providing insight into the active tailoring of the three oscillation modes can be constructed through a single dimensionless number Σ_i[69]:

$$\Sigma_i = \frac{F_v^i}{F_m^i} = \frac{Re_i Sc}{Ma_i}, \tag{10}$$

where the Reynolds number $Re_i = \rho v_i d/\mu$ for the bulk flow estimates the viscous drag force F_v^i, the Marangoni number $Ma_i = \Delta\gamma_i d/\mu D_m$ (where D_m is the molecular diffusivity) for the interfacial flow indicates an estimate of the thermal Marangoni effect, while the Schmidt number $Sc = \mu/\rho D_m$ for liquid properties. The findings not only reveal the underlying intriguing physicochemical hydrodynamics, but also possibly shed light on the 3D bubble manipulation technologies and bubble-based applications.

APPLICATIONS OF PHOTOTHERMAL BUBBLES

To date, bubble-based technologies have shown great promise in diverse areas such as material processing,[106] energy harvest,[107,108] environment treatment,[109] soft-robotics,[10,22] and

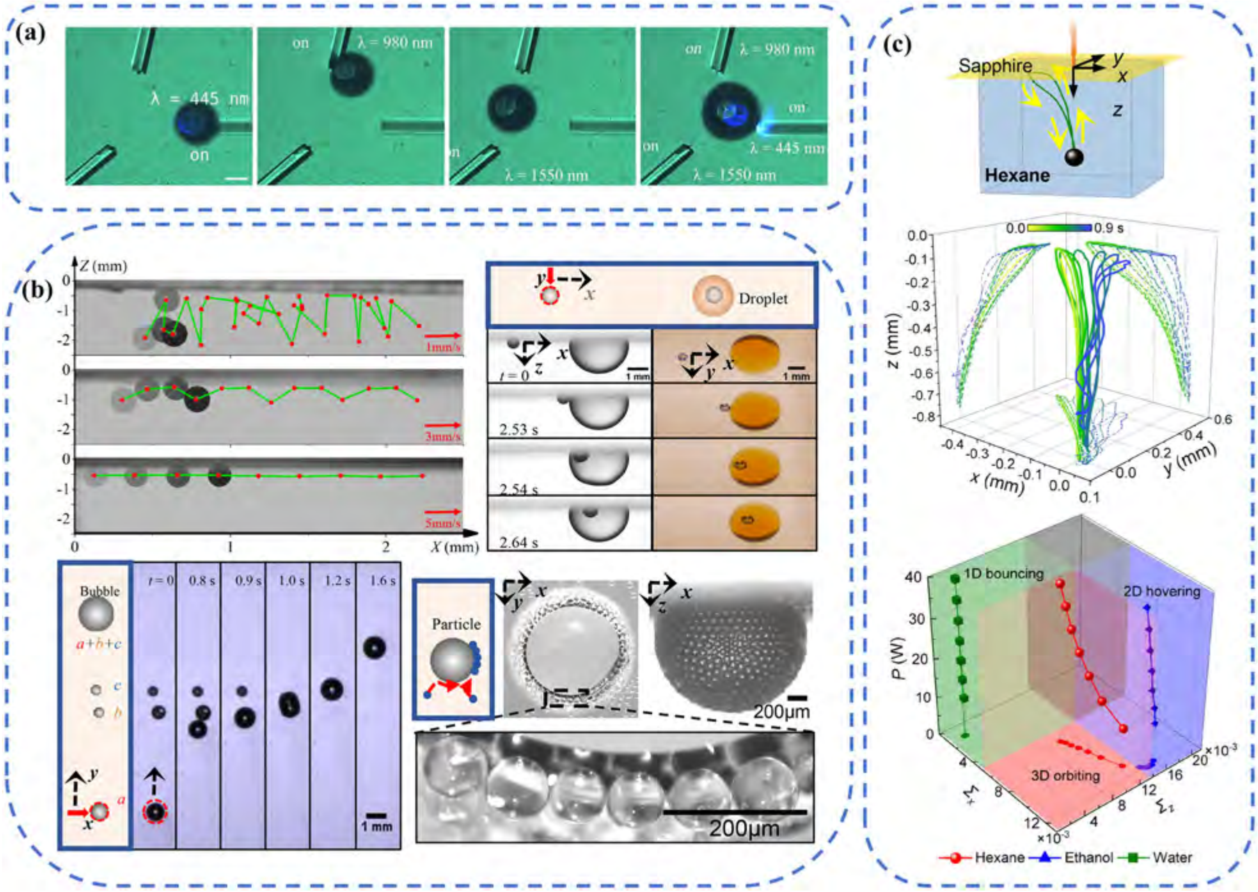

FIGURE 7 3D dancing motion of bubbles via sophisticated designing of laser heating. (a) 3D manipulation and trapping of a bubble due to photothermal effects via sequential laser heating by three optical fibers. Reproduced with permission.[61] Copyright 2021, Optical Society of America. (b) The dancing behavior of a floating photothermal bubble which not only presents the excellent steerability with the laser beam, but also preserves the bouncing behavior along the z vertical direction. The potential application characterizations are also demonstrated. Reproduced with permission.[65] Copyright 2022, Springer Nature. (c) Periodic 3D-orbiting mode of a photothermal bubble in hexane. And a phase diagram of bubble multimode motions in pure liquids is built. Reproduced with permission.[69] Copyright 2025, American Physical Society.

biomedicine.[16,17,72] Herein, we highlight several key applications of photothermal bubbles within microfluidic control, microrobots, microfabrication, and targeted drug delivery.

Photothermal bubbles facilitated liquid control in microfluidic devices

The photothermally generated surface bubbles have been used to manipulate fluids in microfluidic devices, allowing for the development of microfluidic valves or pumps. Zhang et al.[49] demonstrated the function of laser-induced thermal bubbles as in-channel micro-valves and on-spot micro-pumps (Figure 8a). The open/close state of the micro valve can be controlled by the contraction and expansion of the bubble, then the fluid condition can be manipulated in the microchannel. With asymmetric tear-shaped pads, a pumping flow velocity can be controlled by adjusting the laser power, with a variation range of 100–400 μm/s. This bubble technique features simple microfluidic fabrication, high bubble size controllability, freely chosen location, proximity to the point of interest, and easy integration with lab-on-a-chip systems. But, continuous laser heating can damage fragile biological samples. Hence, acoustically oscillating bubbles are typically used as pumps, mixers, or filters for microfluidic aoolications.[9,13,20,112]

Compared with the long lifetime of thermally generated bubble under CW laser irradiating, pulse laser–induced cavitation bubble was used in digital microfluidic devices,[113] where high-speed on-demand droplet generation was achieved. The actuation mechanism of pulse laser–driven droplet generation is based on laser pulse–induced, rapidly expanding cavitation vapor bubbles. When an intense laser pulse is focused in a liquid medium such as water, the strong optical field induces water molecule breakdown which generates a hot plasma at the focal point.[114] The heat quickly dissipates into the medium and creates a rapidly expanding cavitation bubble to perturb the stable oil–water interface and push the neighboring water into the oil channel to form aqueous droplets. The lifetime of a bubble from laser excitation to collapse depends on size and varies from tens to hundreds of microseconds, which enables on-demand droplet generation at rates up to 10,000 droplets per second with precise volume control in a single-layer microfluidic device without any additional on-chip mechanical pumps or valves.

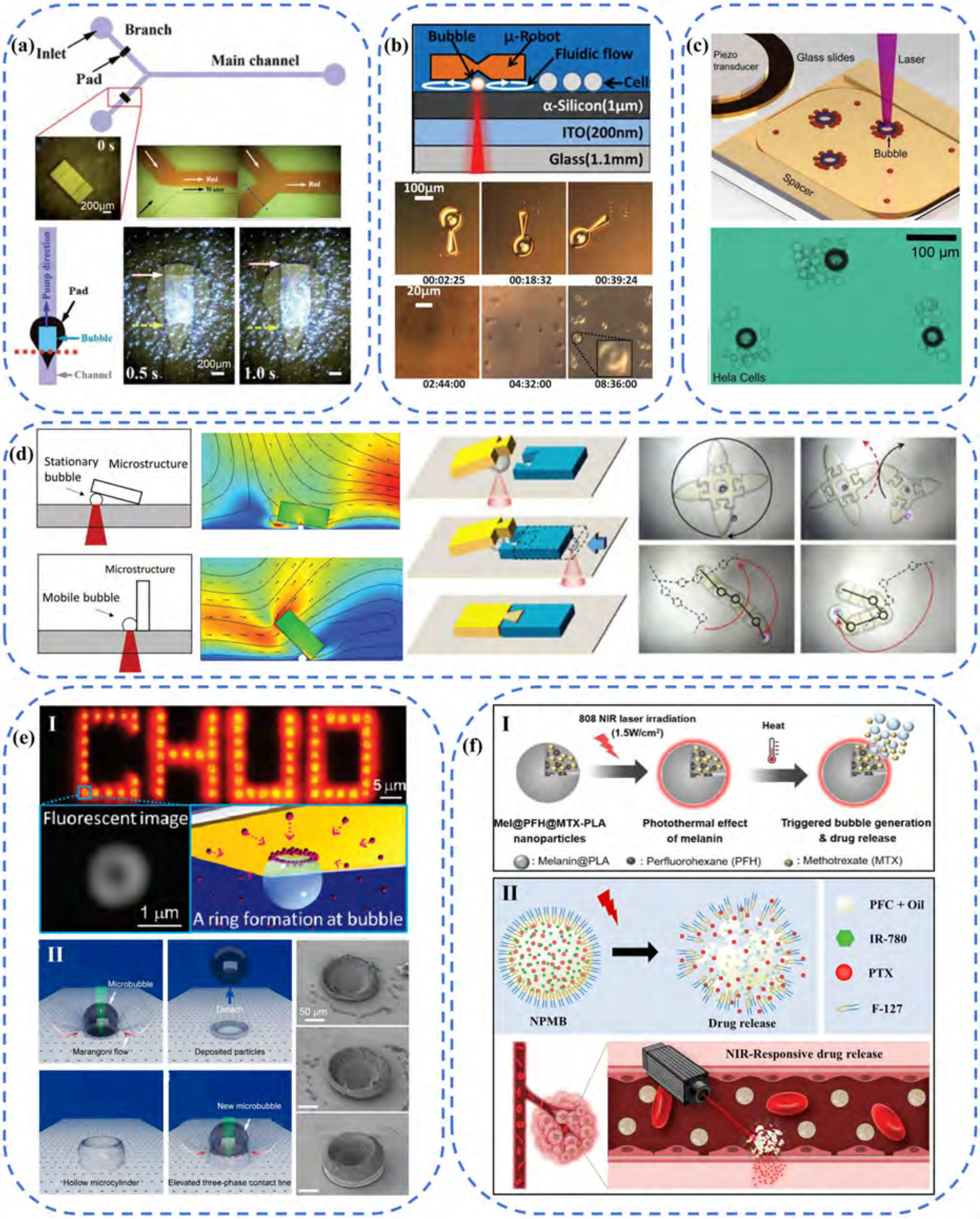

FIGURE 8 Typical applications of photothermal bubbles. (a) A micro-valve and micro-pump based on the photothermal surface bubble. Reproduced with permission.[49] Copyright 2011, Royal Society of Chemistry. (b) Bubble-based hydrogel microrobot system showing the assembly and patterning of cells with an additional manipulation stub. Reproduced with permission.[75] Copyright 2012, Royal Society of Chemistry. (c) "optoacoustic tweezers" utilizing photothermal bubbles as microrobots and combining acoustic radiation forces to trap cell. Reproduced with permission.[89] Copyright 2013, Royal Society of Chemistry. (d) Schematic of plasmonic bubble-assisted assembly of micro-sized modules. Reproduced with permission.[70,77] Copyright 2019, WILEY-VCH GmbH. Copyright 2020, American Chemical Society. (e) Fabrication for ring structure (I) and 3D microcylinder structure (II) of assembled nanoparticles based on laser-induced plasmonic bubbles. Reproduced with permission.[71,79] Copyright 2011, American Chemical Society. Copyright 2024, Elsevier. (f) Bubble-generating drug release platform by irradiating laser on drug loaded nanoparticles (I) or liposome structures (II). Reproduced with permission.[110,111] Copyright 2021, Springer Nature. Copyright 2025, MDPI.

Photothermal bubble–based microrobots

Photothermal bubbles are excellent transporters of mesoscopic objects ranging from metallic nanoparticles[96] to microstructures,[70, 77] due to their convenient manufacturing, easy manipulation, and precise control, which demonstrates their efficacy as a novel tool for micromanipulation. For example, Hu et al.[75] demonstrated a photothermal bubble–based hydrogel microrobot, which allows cell manipulation. The hydrogel structure acts as a buffer between cells and the actuating bubble, reducing shear stress on the cell membrane and avoiding the risk of cell death when directly using the photothermal bubbles due to heating (Figure 8b). Ten separate yeast cells are assembled into an "H" shape by using the bubble-based hydrogel microrobot with an additional manipulation stub, and an assembly of a 3×4 array of agarose microgel blocks is realized.

Another approach to avoid the cells' damage from overheating during the manipulation via photothermal bubbles is to combine the advantages of optical and acoustic method. Xie et al.[89] developed an "optoacoustic tweezers" which utilizes the photothermal effect to generate bubbles in a micro chamber and acoustic radiation forces to trap cells (Figure 8c). By taking advantages of both photothermal bubble generation and acoustic-based trapping mechanism, the integrated technique is capable of creating programmable, complex patterns in a biocompatible manner.

As the 2D operation and assembly of microparticles, cells, or microstructures have been well controlled by the bubble-based microrobots, the demand on 3D manipulation of modules becomes prominent. Wang et al.[115] used the flow field generated by bubble motions to perform a 3D operation upon cell-laden hydrogel micromodules to manufacture biological tissue in vitro. Although the micromodules can realize 3D movement under the action of the flow field, the controllability of the bubbles and micromodules is limited. Moreover, the technology places certain requirements upon the shape of the micromodules, and there must be holes in the center to allow it to be picked up, collected, and aligned. To solve the issue, Dai et al.[70, 77] used a surface photothermal bubble acting as a microrobot to realize the 3D operation and assembly of microstructures (Figure 8d), which provides more opportunities for the construction of biological tissues. With the generation and gradual growth of the photothermal bubble, microstructures can be lifted by the rising convective flow and then rotated in 3D. By changing the position of the light-controlled bubble, the 3D conformations of various microgels can be adjusted.

For bubble-propelled motors, laser-induced vapor flows are adopted to offer the powerful propulsive force to actuate robots. Yang et al.[116] demonstrated the propulsion of a millimeter-sized object by continuously shining a laser on the tail of the light absorber. A vapor jet flow is formed when the photothermal effect is strong enough to convert liquid water into vapor, and a floating paper is propelled. Wang et al.[117] reported a helicopter-like rotary flying photoactuator by using the vapor jet propulsion. Recently, Li et al.[118] proposed a laser-driven bubble-propelled hydrogel microrobot by utilizing an improved photothermal material enhancing the bubble generation ability. With larger bubbles, the movement speeds of the micromotor is significantly increased. Also, the bubble-based microbot can be controlled to achieve a variety of locomotion modes by adjusting the laser parameters.

While bubble-based microrobotics is advancing and demonstrates considerable application potential, substantial challenges persist. Primary concerns encompass the operational stability of photothermal bubbles over extended periods, their controllability in 3D settings, and their capability to accomplish sophisticated assembly operations. Considerable efforts are still required to bridge the gap between technological innovation and practical applications.

Photothermal bubbles mediated microfabrication

Due to the natural hollow structure, bubbles are highly suitable as templates for the fabrication of holow micro-nano structure materials. Fujii et al.[79] demonstrated the fabrication and placement of a ring-like structure of nanoparticles by using a laser-induced thermal bubble on a gold surface (Figure 8e-I). The photothermal bubble acts as a template for the formation of the ring structure. Both Marangoni convection flow and capillary flow around the bubble are responsible for the driving force to assemble nanoparticles into the ring structure from the solution. Due to the feasibility of precise positioning of the ring structure by translating the laser focusing point, various patterns of rings such as arrays and letters and even a double-ring structure can be fabricated without any photomasks or any templates.

Recently, Wang et al.[71] realized the additive manufacturing of 3D microstructures through repetitively nucleated plasmonic bubbles (Figure 8e-II). The dispersed polystyrene microparticles in ethanol are guided by a thermal Marangoni convection flow around the bubble and deposited at the three-phase contact line. By taking advantage of the on/off modulation of laser irradiation, repetitively nucleating and detaching of the plasmonic bubbles are achieved, which facilitates the 3D microstructure fabrication that microparticles can be continuously deposited along the vertical direction to form a 3D hollow microcylinder. This manufacturing method paves the way for 3D microstructure manufacturing by using photothermal bubbles.

Photothermal bubbles in drug delivery

Drug delivery systems, which protect drug molecules during the transport process and release them as required, play a key role in disease therapy. Extensive work have been conducted on targeted drug delivery with the goals of overcoming the limitations of traditional drug therapy and enabling accurate drug delivery and treatment.[119] Using bubbles to achieve targeted drug delivery has attracted increasing attention because of their good drug delivery capacity and stimuli-responsivity.[120, 121]

In recent years, bubble-containing liposomes have been developed for targeted drug/gene delivery. The liposomes usually consist of one or more gas pockets (e.g., air, oxygen, perfluorocarbons) and a flexible covering layer (e.g., lipids, proteins, polymers), and the composition of liposomes can be easily adjusted as required to meet the needs of specific molecules by using different fabrication techniques, such as freeze-lyophilization and reverse phase evaporation methods.[16,17] We focus on bubble-generating liposomes that could generate bubbles in response to the photothermal stimuli. Zhao et al.[122] developed a smart light-responsive liposome for cancer diagnosis and therapy by surface modification. The liposome is coated with a gold shell followed by modification with two kinds of ligands. The drugs are encapsulated in the liposome. Once the liposome adheres to tumor cells through the binding between the ligands on liposome surfaces and receptors on tumor cell surfaces, the position and size of the tumor can be easily diagnosed. NIR irradiation triggers the decomposition of the liposomal drugs, generating CO_2 bubbles that disrupt the lipid structure and release the drugs. Meanwhile, the photothermal effect of the gold shell also enhances tumor cell killing.

Different from the generation of bubbles through chemical decomposition reaction mediated by the laser heating, photothermal bubbles can be directly generated to control drug release. Lee et al.[110] developed a thermo-responsive bubble-generating drug release platform by irradiating NIR laser on drug loaded nanoparticles (Mel@PFH@MTX-PLA) (Figure 8f-I). Here, melanin acts as the laser-absorbing material and generates heat once it is irradiated. The temperature increase could cause the phase transition of perfluorohexane (PFH), resulting in dramatic bubble generation, which triggers the drug (Methotrexate) release. Recently, Kim et al.[111] also proposed an NIR-responsive microbubble delivery platform for controlled drug release in cancer therapy (Figure 8f-II). The system consists of an oil phase, 2H,3H-perfluoropentane (PFC), a photosensitizer (IR-780), and an anticancer drug. In the absence of laser stimulation, IR-780 and the drug coexist in oil and PFC to maintain a stable microbubble (liposome) state. Once IR-780 absorbs the NIR light, PFC undergoes a phase change from liquid to gas, which induces the liposome expansion and collapses, thereby facilitating efficient drug delivery in the body. This system combines photothermal effects and bubble dynamics to enable precisely controlled drug release, which may overcome nonspecific drug release and enable localized, targeted anticancer therapy with minimal side effects.

In addition to drug delivery, laser-induced cavitation bubbles show promise in suppressing tumor growth and spread. This capability stems from the destructive shock waves and microjets produced during bubble collapse, which can kill tumor cells or facilitate drug uptake by penetrating vascular or cellular barriers.[123,124] Despite progress in bubble-assisted therapy, enhancing the robustness and biocompatibility of these systems continues to be a key challenge.

SUMMARY AND OUTLOOK

In this review, we have provided an overview of the advances in photothermal bubble research over the last 10 years, from the fundamentals of nucleation and growth dynamics under localized laser heating to the multi-mode manipulation techniques enabled by photothermal effects, as well as their associated applications. Although photothermal bubbles offer unique capabilities due to their intense, localized, and rapid energy conversion, and have opened up a novel path for the development of microfabrication,[125] micromanipulation,[70] robot propulsion,[126] and clinical therapy,[123] the inherent complexity of bubble dynamics and manipulations present substantial challenges that hinder widespread, reliable, and scalable implementation.

The inherent instability, chaotic dynamics, and sensitivity to environmental conditions constrain practical applications of photothermal bubbles. For instance, the nucleation, growth, and collapse of bubbles, together with the associated flows (e.g., microstreaming and jetting), rely on laser parameters (e.g., power, pulse duration, and focus),[127] material properties (e.g., absorption coefficient, viscosity, and surface tension),[69] and local environment (e.g., contaminants and dissolved gases),[78,128] complicating the bubble dynamics. For bubble manipulation, precise control of bubble motions in 3D paths remains extremely challenging. For applications, the intense localized heat may cause the transferred material or the substrate to undergo unintended thermal modification, melting, or decomposition, especially for biological materials.[129] And, the high shear forces generated by microstreaming and the shockwaves/pressure spikes resulting from bubble collapse can lyse or severely damage fragile cells, thereby limiting their utility in live cell sorting or analysis.[130]

To overcome these challenges, multidisciplinary efforts are required. For example, advanced models or simulations should be developed by considering the effect of light absorption, heat transfer, fluid dynamics, and bubble mechanisms, to precisely predict the bubble motion. Novel materials and structures need to be further investigated, such as slippery surface,[45,131] engineering photothermal absorbers with higher efficiency, improved stability, and biocompatibility. Furthermore, employing coordinated control via hybrid physical fields or multi-physical-field is promising. For instance, to mitigate the risk of cellular damage caused by localized laser heating in photothermal bubble microrobots, acoustic fields were integrated with photothermal excitation where laser-induced microbubbles were generated near target cells, and their motion was then precisely controlled via acoustic waves, enabling efficient, non-contact cell manipulation with high biocompatibility.[132] Similarly, optoelectronic tweezers and optoacoustic tweezers have been successfully applied in micro/nano-manipulation.[89,98,133,134] These advancements suggest that multi-physical-field synergy will serve as a foundational strategy for future functional integration in bubble-based technologies.

ACKNOWLEDGMENTS

This work was supported by National Natural Science Foundation of China (Grant Number 12572307), Shanghai Science and Technology Program (Grant Number 23ZR1403800); F. W. acknowledges funding support from the Postdoctoral Fellowship Program of the China Postdoctoral Science Foundation (Grant Numbers 2025T180524, GZB20240366, and 2024M751637), and Shuimu Tsinghua Scholar Program (Grant Number 2023SM038).

CONFLICT OF INTEREST STATEMENT

The authors declare no conflicts of interest.

ORCID

Man Hu https://orcid.org/0000-0002-4623-3155
Feng Wang https://orcid.org/0000-0003-0025-3895
Daosheng Deng https://orcid.org/0000-0002-4203-5119

REFERENCES

1. Lohse D. Bubble puzzles: from fundamentals to applications. *Phys Rev Fluids*. 2018; 3: 110504.
2. Legendre D, Zenit R. Gas bubble dynamics. *Rev Mod Phys*. 2025; 97: 025001.
3. Rodríguez-Rodríguez J, Sevilla A, Martínez-Bazán C, Gordillo JM. Generation of microbubbles with applications to industry and medicine. *Annu Rev Fluid Mech*. 2015; 47: 405-429.
4. Liang X, Kumar V, Ahmadi F, Zhu Y. Manipulation of droplets and bubbles for thermal applications. *Droplet*. 2022; 1: 80-91.
5. Guan N, Wang Y, Hu J, Zhang L. Micro-nano bubbles: a new field of eco-friendly cleaning. *Nanomaterials*. 2025; 15: 480.
6. Zhou A, Zhao Y, Ding X, Wu X, Li P. Eco-friendly textile cleaning: micro-nano bubbles technology for enhanced efficiency and sustainability. *J Text Inst*. 2024; 116: 2022-2030.
7. Wang H, Yang W, Yan X, Wang L, Wang Y, Zhang H. Regulation of bubble size in flotation: a review. *J Environ Chem Eng*. 2020; 8: 104070.
8. Jung MU, Kim YC, Bournival G, Ata S. Industrial application of microbubble generation methods for recovering fine particles through froth flotation: a review of the state-of-the-art and perspectives. *Adv Colloid Interface Sci*. 2023; 322: 103047.
9. Li Y, Liu X, Huang Q, Ohta AT, Arai T. Bubbles in microfluidics: an all-purpose tool for micromanipulation. *Lab Chip*. 2021; 21: 1016-1035.
10. Zhou Y, Dai L, Jiao N. Review of bubble applications in microrobotics: propulsion, manipulation, and assembly. *Micromachines*. 2022;13: 1068.
11. Visser CW, Amato DN, Mueller J, Lewis JA. Polymer foams: architected polymer foams via direct bubble writing. *Advanced Materials*. 2019; 31: 1970326.
12. Amato DN, Amato DV, Sandoz M, Weigand J, Patton DL, Visser CW. Programmable porous polymers via direct bubble writing with surfactant-free inks. *ACS Appl Mater Interfaces*. 2020; 12: 42048-42055.
13. Hashmi A, Yu G, Reilly-Collette M, Heiman G, Xu J. Oscillating bubbles: a versatile tool for lab on a chip applications. *Lab Chip*. 2012; 12: 4216-4227.
14. Oskooei A, Günther A. Bubble pump: scalable strategy for in-plane liquid routing. *Lab Chip*. 2015; 15: 2842-2853.
15. Huang C, Tsou C. The implementation of a thermal bubble actuated microfluidic chip with microvalve, micropump and micromixer. *Sens Actuators A Phys*. 2014; 210: 147-156.
16. Huang SL. Liposomes in ultrasonic drug and gene delivery. *Adv Drug Delivery Rev*. 2008; 60: 1167-1176.
17. Chen K-J, Liang H-F, Chen H-L, et al. A thermoresponsive bubble-generating liposomal system for triggering localized extracellular drug delivery. *ACS Nano*. 2013; 7: 438-446.
18. Wu Z, Li L, Yang Y, et al. A microrobotic system guided by photoacoustic computed tomography for targeted navigation in intestines in vivo. *Sci Rob*. 2019; 4: eaax0613.
19. Sánchez S, Soler L, Katuri J. Chemically powered micro- and nanomotors. *Angew Chem Int Ed*. 2015; 54: 1414-1444.
20. Segers T, Versluis M. Acoustic bubble sorting for ultrasound contrast agent enrichment. *Lab Chip*. 2014; 14: 1705-1714.
21. Stride E, Segers T, Lajoinie G, et al. Microbubble agents: new directions. *Ultrasound Med Biol*. 2020; 46: 1326-1343.
22. Wang W, He Y, Liu H, Guo Q, Ge Z, Yang W. Bubble-based microrobot: recent progress and future perspective. *Sens Actuators, A*. 2023; 360: 114567.
23. Li X, Zhang J, Wang X, et al. Bio-inspired spontaneous splitting of underwater bubbles along a superhydrophobic open pathway without perturbation. *Droplet*. 2022; 1: 65–75.
24. O'Coin D, Ling H. Effect of gas flow rate on bubble formation on superhydrophobic surface. *Droplet*. 2025; 4: e148.
25. Gao Y, Wu M, Lin Y, Xu J. Trapping and control of bubbles in various microfluidic applications. *Lab Chip*. 2020; 20: 4512-4527.
26. Lin F, Wo K, Fan X, Wang W, Zou J. Directional transport of underwater bubbles on solid substrates: principles and applications. *ACS Appl Mater Interfaces*. 2023; 15: 10325-10340.
27. Yu C, Zhang P, Wang J, Jiang L. Superwettability of gas bubbles and its application: from bioinspiration to advanced materials. *Adv Mater*. 2017; 29: 1703053.
28. Zhu S, Bian Y, Wu T, et al. Spontaneous and unidirectional transportation of underwater bubbles on superhydrophobic dual rails. *Appl Phys Lett*. 2020; 116: 093706.
29. Xu Y, Hashmi A, Yu G, et al. Microbubble array for on-chip worm processing. *Appl Phys Lett*. 2013; 102: 023702.
30. Liu D, Wang Y, Chen W, et al. Bubble manipulation mediated by external stimuli: from bioinspired design to potential applications. *Nano Today*. 2024; 55: 102177.
31. Ahmed D, Ozcelik A, Bojanala N, et al. Rotational manipulation of single cells and organisms using acoustic waves. *Nat Commun*. 2016; 7: 11085.
32. Zhang W, Song B, Bai X, et al. Versatile acoustic manipulation of micro-objects using mode-switchable oscillating bubbles: transportation, trapping, rotation, and revolution. *Lab Chip*. 2021; 21: 4760-4771.
33. Läubli NF, Shamsudhin N, Vogler H, et al. 3D manipulation and imaging of plant cells using acoustically activated microbubbles. *Small Methods*. 2019; 3: 1800527.
34. Chen H, Hong Z, Zang D. New insights into suspended drops: when soft matter meets acoustic levitation. *Droplet*. 2024; 3: e95.
35. Yan Y, Guo Z, Zhang X, et al. Electrowetting-induced stiction switch of a microstructured wire surface for unidirectional droplet and bubble motion. *Adv Funct Mater*. 2018; 28: 1800775.
36. Zhao Y, Cho SK. Micro air bubble manipulation by electrowetting on dielectric (EWOD): transporting, splitting, merging and eliminating of bubbles. *Lab Chip*. 2007; 7: 273-280.
37. Guo P, Wang Z, Heng L, Zhang Y, Wang X, Jiang L. Magnetocontrollable droplet and bubble manipulation on a stable amphibious slippery gel surface. *Adv Funct Mater*. 2019; 29: 1808717.
38. Zhu S, Bian Y, Wu T, et al. High performance bubble manipulation on ferrofluid-infused laser-ablated microstructured surfaces. *Nano Lett*. 2020; 20: 5513-5521.
39. Jiang S, Wu D, Li J, Chu J, Hu Y. Magnetically responsive manipulation of droplets and bubbles. *Droplet*. 2024; 3: e117.
40. Wang L, Chen L, Zheng X, et al. Multimodal bubble microrobot near an air–water interface. *Small*. 2022; 18: 2203872.
41. Molina-Jiménez JM, Morales-Cruzado B, Briceão-Ahumada Z, Carrasco-Fadanelli V, Sarmiento-Gómez E. Trapping and manipulation of bubbles with holographic optical tweezers. *Soft Matter*. 2024; 20: 2032-2039.
42. Ito M, Mayama H, Asaumi Y, Nakamura Y, Fujii S. Light-driven locomotion of bubbles. *Langmuir*. 2020; 36: 7021-7031.
43. Zhao L, Seshadri S, Liang X, et al. Depinning of multiphase fluid using light and photo-responsive surfactants. *ACS Cent Sci*. 2022; 8: 235-245.
44. Chen C, Huang Z, Shi L-A, et al. Remote photothermal actuation of underwater bubble toward arbitrary direction on planar slippery Fe_3O_4-doped surfaces. *Adv Funct Mater*. 2019; 29: 1904766.

45. Qian C, Chen Z, Meng X, Li Q, Chen X. Directional droplet/bubble transportation on slippery photothermal responsive laser-induced graphene/polyimide membrane. *Chem Eng J*. 2023; 469: 143819.
46. Chiou P-Y, Chang Z, Wu MC. Droplet manipulation with light on optoelectrowetting device. *J Microelectromech Syst*. 2008; 17: 133-138.
47. Baigl D. Photo-actuation of liquids for light-driven microfluidics: state of the art and perspectives. *Lab Chip*. 2012; 12: 3637-3653.
48. Zhang Q, Pang Y, Schiffbauer J, et al. Light-guided surface plasmonic bubble movement via contact line de-pinning by in-situ deposited plasmonic nanoparticle heating. *ACS Appl Mater Interfaces*. 2019; 11: 48525-48532.
49. Zhang K, Jian A, Zhang X, Wang Y, Li Z, Tam Hy. Laser-induced thermal bubbles for microfluidic applications. *Lab Chip*. 2011; 11: 1389-1395.
50. Sarabia-Alonso JA, Ramos-García R. Optothermal generation, steady-state trapping, and 3D manipulation of bubbles: an experimental and theoretical analysis of the Marangoni effect. *J Opt*. 2024; 26: 083501.
51. Xie Y, Zhao C. An optothermally generated surface bubble and its applications. *Nanoscale*. 2017; 9: 6622-6631.
52. Zhang C-L, Wang Y-Q, Gong Y, Wu Y, Peng G-D, Rao Y-J. The generation and assembly of laser-induced microbubbles. *J Lightwave Technol*. 2018; 36: 2492-2498.
53. Li B-W, He J-W, Bai W, Wang H-D, Ji F, Zhong M-C. An approach of bubble generation and manipulation by using the photothermal effects of laser irradiation on light absorbing particles. *Rev Sci Instrum*. 2021; 92: 114902.
54. Setoura K, Ito S, Miyasaka H. Stationary bubble formation and Marangoni convection induced by CW laser heating of a single gold nanoparticle. *Nanoscale*. 2017; 9: 719-730.
55. Young NO, Goldstein JS, Block MJ. The motion of bubbles in a vertical temperature gradient. *J Fluid Mech*. 1959; 6: 350-356.
56. Nath S, Ricard G, Jin P, Bouillant A, Quéré D. Thermal Marangoni bubbles. *Soft Matter*. 2022; 18: 7422-7426.
57. Wei Z, Wang H, Chen Y, Xing J, Li D. Microbubble/droplet manipulation based on Marangoni effect. *Prog Chem*. 2024; 36: 1541-1558.
58. Ma Y, Cheng Y, Shen Y, Xu J, Sui Y. Manipulation of bubble migration through thermal capillary effect under variable buoyancy. *Int J Therm Sci*. 2020; 149: 106199.
59. Ohta AT, Jamshidi A, Valley JK, Hsu H-Y, Wu MC. Optically actuated thermocapillary movement of gas bubbles on an absorbing substrate. *Appl Phys Lett*. 2007; 91: 074103.
60. Li X, Wang F, Xia C, The HL, Bomer JG, Wang Y. Laser controlled manipulation of microbubbles on a surface with silica-coated gold nanoparticle array. *Small*. 2023; 19: 2302939.
61. Sarabia-Alonso JA, Ortega-Mendoza JG, Mansurova S, Munoz-Pérez FM, Ramos-García R. 3D trapping of microbubbles by the Marangoni force. *Opt Lett*. 2021; 46: 5786-5789.
62. Rahman MA, Cheng J, Wang Z, Ohta AT. Cooperative micromanipulation using the independent actuation of fifty microrobots in parallel. *Sci Rep*. 2017; 7: 3278.
63. Baffou G, Polleux J, Rigneault H, Monneret S. Super-heating and micro-bubble generation around plasmonic nanoparticles under CW illumination. *J Phys Chem C*. 2014; 118: 4890-4898.
64. Pimentel-Domínguez R, Hernández-Cordero J, Zenit R. Microbubble generation using fiber optic tips coated with nanoparticles. *Opt Express*. 2012; 20: 8732-8740.
65. Hu M, Wang F, Chen L, et al. Near-infrared-laser-navigated dancing bubble within water via a thermally conductive interface. *Nat Commun*. 2022; 13: 5749.
66. Hu W, Fan Q, Ohta AT. Interactive actuation of multiple optothermocapillary flow-addressed bubble microrobots. *Robot Biomim*. 2014; 1: 14.
67. Lin L, Peng X, Mao Z, et al. Bubble-pen lithography. *Nano Lett*. 2016; 16: 701-708.
68. Zeng B, Chong KL, Wang Y, et al. Periodic bouncing of a plasmonic bubble in a binary liquid by competing solutal and thermal Marangoni forces. *Proc Natl Acad Sci USA*. 2021; 118: e2103215118.
69. Hu M, Wang F, Li Y, et al. 3D periodic orbiting of a photothermal bubble. *Phys Rev Lett*. 2025; 134: 104004.
70. Dai L, Ge Z, Jiao N, Liu L. 2D to 3D manipulation and assembly of microstructures using optothermally generated surface bubble microrobots. *Small*. 2019; 15: 1902815.
71. Wang F, Dong L, Wang Z, et al. Additive manufacturing of 3D surface microstructures through repetitively nucleated plasmonic bubbles. *Surf Interfaces*. 2024; 44: 103710.
72. Qiao C, Yang D, Mao X, et al. Recent advances in bubble-based technologies: underlying interaction mechanisms and applications. *Appl Phys Rev*. 2021; 8: 011315.
73. Wang F, Wang Z, Dong L, Liu H, Yang L, Wang Y. Plasmonic bubbles: from fundamentals to applications. *Adv Funct Mater*. 2024; 34: 2403606.
74. Zheng Y, Liu H, Wang Y, et al. Accumulating microparticles and direct-writing micropatterns using a continuous-wave laser-induced vapor bubble. *Lab Chip*. 2011; 11: 3816-3820.
75. Hu W, Ishii KS, Fan Q, Ohta AT. Hydrogel microrobots actuated by optically generated vapour bubbles. *Lab Chip*. 2012; 12: 3821-3826.
76. Zhao C, Xie Y, Mao Z, et al. Theory and experiment on particle trapping and manipulation via optothermally generated bubbles. *Lab Chip*. 2014; 14: 384-391.
77. Dai L, Lin D, Wang X, Jiao N, Liu L. Integrated assembly and flexible movement of microparts using multifunctional bubble microrobots. *ACS Appl Mater Interfaces*. 2020; 12: 57587-57597.
78. Wang Y, Zaytsev ME, The HL, et al. Vapor and gas-bubble growth dynamics around laser-irradiated, water-immersed plasmonic nanoparticles. *ACS Nano*. 2017; 11: 2045-2051.
79. Fujii S, Kanaizuka K, Toyabe S, Kobayashi K, Muneyuki E, Haga Ma. Fabrication and placement of a ring structure of nanoparticles by a laser-induced micronanobubble on a gold surface. *Langmuir*. 2011; 27: 8605-8610.
80. Ortega-Mendoza JG, Sarabia-Alonso JA, Zaca-Morán P, et al. Marangoni force-driven manipulation of photothermally-induced microbubbles. *Opt Express*. 2018; 26: 6653-6662.
81. Hu M, Li Y, Chen L, et al. A hovering bubble with a spontaneous horizontal oscillation. *Proc Natl Acad Sci USA*. 2024; 121: e2413880121.
82. Brennen CE. *Cavitation and Bubble Dynamics*. Cambridge University Press; 2013.
83. Plesset MS, Prosperetti A. Bubble dynamics and cavitation. *Annu Rev Fluid Mech*. 1977; 9: 145-185.
84. Prosperetti A. Vapor bubbles. *Annu Rev Fluid Mech*. 2017; 49: 221-248.
85. Plesset MS, Zwick S. A nonsteady heat diffusion problem with spherical symmetry. *J Appl Phys*. 1952; 23: 95-98.
86. Plesset MS, Zwick SA. The growth of vapor bubbles in superheated liquids. *J Appl Phys*. 1954; 25: 493-500.
87. Cho HJ, Wang EN. Bubble nucleation, growth, and departure: a new, dynamic understanding. *Int J Heat Mass Transfer*. 2019; 145: 118803.
88. Huang W, Zhao L, He X, et al. Low-temperature Leidenfrost-like jumping of sessile droplets on microstructured surfaces. *Nat Phys*. 2024; 20: 1274-1281.
89. Xie Y, Zhao C, Zhao Y, et al. Optoacoustic tweezers: a programmable, localized cell concentrator based on opto-thermally generated, acoustically activated, surface bubbles. *Lab Chip*. 2013; 13: 1772-1779.
90. Lohse D, Zhang X. Surface nanobubbles and nanodroplets. *Rev Mod Phys*. 2015; 87: 981-1035.
91. Nicholson JW, Windeler RS, DiGiovanni DJ. Optically driven deposition of single-walled carbon-nanotube saturable absorbers on optical fiber end-faces. *Opt Express*. 2007; 15: 9176-9183.

92. Kashiwagi K, Yamashita S, Set SY. Optically manipulated deposition of carbon nanotubes onto optical fiber end. *Japanese J Appl Phys*. 2007; 46: L988.
93. Munoz-Perez FM, Ortega-Mendoza JG, Padilla-Vivanco A, Toxqui-Quitl C, Sarabia-Alonso JA, Ramos-Garcia R. Steady-state 3D trapping and manipulation of microbubbles using thermocapillary. *Front Phys*. 2020; 8: 585590.
94. Sarabia-Alonso J, Pérez-Corte J, Ortega-Mendoza J, et al. Self-oscillation of 3D trapped bubbles. *Opt Laser Technol*. 2024; 172: 110509.
95. Hu W, Ishii KS, Ohta AT. Micro-assembly using optically controlled bubble microrobots. *Appl Phys Lett*. 2011; 99: 094103.
96. Ghosh S, Ranjan AD, Das S, et al. Directed self-assembly driven mesoscale lithography using laser-induced and manipulated microbubbles: complex architectures and diverse applications. *Nano Lett*. 2021; 21: 10-25.
97. Kollipara PS, Mahendra R, Li J, Zheng Y. Bubble-pen lithography: fundamentals and applications. *Aggregate*. 2022; 3: e189.
98. Chiou P, Ohta A, Wu M. Massively parallel manipulation of single cells and microparticles using optical images. *Nature*. 2005; 436: 370-372.
99. Porfirev A. Spatial-light-modulator-assisted laser manipulation in air. *Opt Eng*. 2020; 59: 055109.
100. Mio C, Gong T, Terray A, Marr DWM. Design of a scanning laser optical trap for multiparticle manipulation. *Rev Sci Instrum*. 2000; 71: 2196-2200.
101. Cao Z, Feng Y, Zhang B, Xu Q, Wang Y, Guo L. Regulation of bubble behavior on a TiO2 photoelectrode surface during photoelectrocatalytic water splitting. *J Phys Chem C*. 2022; 126: 12480-12491.
102. Yan X, Xu J, Meng Z, Xie J, Wang H. A new mechanism of light-induced bubble growth to propel microbubble piston engine. *Small*. 2020; 16: 2001548.
103. Park S, Liu L, Demirkır, et al. Solutal Marangoni effect determines bubble dynamics during electrocatalytic hydrogen evolution. *Nat Chem*. 2023; 15: 1532-1540.
104. Angulo A, van der Linde P, Gardeniers H, Modestino M, Fernández Rivas D. Influence of bubbles on the energy conversion efficiency of electrochemical reactors. *Joule*. 2020; 4: 555-579.
105. Li J, Xu Q, Luo X, et al. Size effects on bubble dynamics during photoelectrochemical water splitting. *ACS Nano*. 2025; 19: 8200-8211.
106. Feng J, Nunes JK, Shin S, et al. A scalable platform for functional nanomaterials via bubble-bursting. *Adv Mater*. 2016; 28: 4047-4052.
107. Yan X, Xu W, Deng Y, et al. Bubble energy generator. *Sci Adv*. 2022; 8: eabo7698.
108. Wang D, Liu Z, Zhao H, et al. Launching by cavitation. *Science*. 2025; 389: 935-939.
109. Temesgen T, Bui TT, Han M, Kim iT, Park H. Micro and nanobubble technologies as a new horizon for water-treatment techniques: a review. *Adv Colloid Interface Sci*. 2017; 246: 40-51.
110. Lee H, Kim MA, Lee CM. Near-infrared laser-responsive photothermal bubble-generating PLA nanoparticles for controlled drug release. *Macromol Res*. 2021; 29: 224-229.
111. Kim K, Yoon B, Lee J, Kim G, Park MH. NIR-responsive microbubble delivery platforms for controlled drug release in cancer therapy. *Materials*. 2025; 18: 2725.
112. Bertin N, Spelman TA, Combriat T, et al. Bubble-based acoustic micropropulsors: active surfaces and mixers. *Lab Chip*. 2017; 17: 1515-1528.
113. Park SY, Wu TH, Chen Y, Teitell MA, Chiou PY. High-speed droplet generation on demand driven by pulse laser-induced cavitation. *Lab Chip*. 2011; 11: 1010-1012.
114. Dijkink R, Ohl CD. Laser-induced cavitation based micropump. *Lab Chip*. 2008; 8: 1676-1681.
115. Wang H, Cui J, Zheng Z, et al. Assembly of RGD-modified hydrogel micromodules into permeable three-dimensional hollow microtissues mimicking in vivo tissue structures. *ACS Appl Mater Interfaces*. 2017; 9: 41669-41679.
116. Yang R-L, Zhu Y-J, Qin D-D, Xiong Z-C. Light-operated dual-mode propulsion at the liquid/air interface using flexible, superhydrophobic, and thermally stable photothermal paper. *ACS Appl Mater Interfaces*. 2020; 12: 1339-1347.
117. Wang D, Chen Z, Li M, et al. Bioinspired rotary flight of light-driven composite films. *Nat Commun*. 2023; 14: 2070.
118. Li M, Wang P, Zhang H, et al. Manipulation study of bubble-propelled hydrogel microbots. *Adv Mater Technologies*. 2025; 10: 2401265.
119. Zhang Y, Chan HF, Leong KW. Adv Mater and processing for drug delivery: the past and the future. *Adv Drug Delivery Rev*. 2013; 65: 104-120.
120. Park J, Kim Y, Jeong J, Jang D, Kim D, Chung S. Acoustic bubble and magnetic actuation-based microrobot for enhanced multiphase drug delivery efficiency. *Micromachines*. 2023;14: 2169.
121. Klibanov AL, Shevchenko TI, Raju BI, Seip R, Chin CT. Ultrasound-triggered release of materials entrapped in microbubble–liposome constructs: a tool for targeted drug delivery. *J Controlled Release*. 2010; 148: 13-17.
122. Zhao F, Zhou J, Su X, et al. A smart responsive dual aptamers-targeted bubble-generating nanosystem for cancer triplex therapy and ultrasound imaging. *Small*. 2017; 13: 1603990.
123. Shao J, Xuan M, Dai L, Si T, Li J, He Q. Near-infrared-activated nanocalorifiers in microcapsules: vapor bubble generation for in-vivo enhanced cancer therapy. *Angew Chem Int Ed*. 2015; 54: 12782-12787.
124. Xiang G, Chen J, Ho D, et al. Shock waves generated by toroidal bubble collapse are imperative for kidney stone dusting during Holmium:YAG laser lithotripsy. *Ultrason Sonochem*. 2023; 101: 106649.
125. Armon N, Greenberg E, Edri E, Nagler-Avramovitz O, Elias Y, Shpaisman H. Laser-based printing: from liquids to microstructures. *Adv Funct Mater*. 2021; 31: 2008547.
126. Zhan Z, Wei F, Zheng J, Yang W, Luo J, Yao L. Recent advances of light-driven micro/nanomotors: toward powerful thrust and precise control. *Nanotechnol Rev*. 2018; 7: 555-581.
127. Kim N, Park H, Do H. Evolution of cavitation bubble in tap water by continuous-wave laser focused on a metallic surface. *Langmuir*. 2019; 35: 3308-3318.
128. Hu M, Wang F, Huo P, et al. Nanoparticle-mediated cavitation via CO2 laser impacting on water: concentration effect, temperature visualization, and core-shell structures. *Sci Rep*. 2019; 9: 18326.
129. Vogel A, Venugopalan V. Mechanisms of pulsed laser ablation of biological tissues. *Chem Rev*. 2003; 103: 2079-2079.
130. Preso D, Fuster D, Sieber A, Obreschkow D, Farhat M. Vapor compression and energy dissipation in a collapsing laser-induced bubble. *Phys Fluids*. 2024;36: 033342.
131. Zhan H, Yuan Z, Li Y, et al. Versatile bubble maneuvering on photopyroelectric slippery surfaces. *Nat Commun*. 2023; 14: 6158.
132. Xie Y, Nama N, Li P, et al. Probing cell deformability via acoustically actuated bubbles. *Small*. 2016; 12: 902-910.
133. Zhang S, Xu B, Elsayed M, et al. Optoelectronic tweezers: a versatile toolbox for nano-/micro-manipulation. *Chem Soc Rev*. 2022; 51: 9203-9242.
134. Ozcelik A, Rufo J, Guo F, et al. Acoustic tweezers for the life sciences. *Nat Methods*. 2018; 15: 1021-1028.

How to cite this article: Hu M, Wang F, Deng D. Photothermal bubble: Dynamics, manipulation, and applications. *Droplet*. 2026;e70071. https://doi.org/10.1002/dro2.70071